SMAI-JCM
SMAI Journal of Computational Mathematics

Unique continuation for an elliptic interface problem using unfitted isoparametric finite elements

Erik Burman & Janosch Preuss

Volume 11 (2025), p. 165-202.
https://doi.org/10.5802/smai-jcm.122

The SMAI Journal of Computational Mathematics is a member of the Centre Mersenne for Open Scientific Publishing
http://www.centre-mersenne.org/
Submissions at https://smai-jcm.centre-mersenne.org/ojs/submission
e-ISSN: 2426-8399

SMAI Journal of Computational Mathematics
Vol. 11, 165-202 (2025)

Unique continuation for an elliptic interface problem using unfitted isoparametric finite elements

Erik Burman [1]
Janosch Preuss [2]

[1] Department of Mathematics, University College London, United Kingdom
E-mail address: e.burman@ucl.ac.uk
[2] Department of Mathematics, University College London, United Kingdom
E-mail address: janosch.preuss@inria.fr.

Abstract. We study unique continuation over an interface using a stabilized unfitted finite element method tailored to the conditional stability of the problem. The interface is approximated using an isoparametric transformation of the background mesh and the corresponding geometrical error is included in our error analysis. To counter possible destabilizing effects caused by non-conformity of the discretization and cope with the interface conditions, we introduce adapted regularization terms. This allows to derive error estimates based on conditional stability. The necessity and effectiveness of the regularization is illustrated in numerical experiments. We also explore numerically the effect of the heterogeneity in the coefficients on the ability to reconstruct the solution outside the data domain. For Helmholtz equations we find that a jump in the flux impacts the stability of the problem significantly less than the size of the wavenumber.

2020 Mathematics Subject Classification. 35J15, 65N12, 65N20, 65N30, 86-08.

Keywords. unfitted finite element method, unique continuation, interface problems, isoparametric finite element method, geometry errors, conditional Hölder stability.

1. Introduction

1.1. Motivation

Recently, there has been an increasing interest in the development of numerical methods for unique continuation problems, see e.g. [5, 8, 10, 14, 15, 23, 39]. These methods are based on so called conditional stability estimates which represent a quantitative form of the unique continuation property for solutions of certain partial differential equations (PDEs). In addition, many physical applications involve interfaces over which material parameters can exhibit jump discontinuities, e.g. in seismic wave propagation. Despite the practical relevance of these problems, numerical methods for unique continuation involving interfaces seem to be unavailable in the literature.

On the other hand, the development of numerical methods, e.g. finite elements methods (FEMs), for well-posed problems involving interfaces is well advanced. So called unfitted FEMs are very appealing to treat these problems, see e.g. [7, 9, 22, 30, 34, 38, 46, 47, 48], since they allow the use of simple meshes which are independent of the possibly complex geometry of the interface. However, the analysis and implementation of unfitted FEMs imposes some challenges (stability of variational formulations, usually only an implicit description of the geometry is available, ...) which are poorly understood in the context of ill-posed problems. In this paper, we make some progress in this direction by developing an unfitted FEM for a unique continuation problem involving an interface.

This work was funded EPSRC grant EP/V050400/1.
https://doi.org/10.5802/smai-jcm.122

1.2. **The problem setting**

We define the problem setting as sketched in Figure 1.1. Let $\Omega \subset \mathbb{R}^d, d \in \{2,3\}$, be a bounded, connected and open set split by a smooth interface Γ into two connected components Ω_1 and Ω_2 such that $\Gamma = \partial\Omega_1$ and $\Omega = \Omega_1 \cup \Gamma \cup \Omega_2$. Given the functions u_i on Ω_i, we identify u on $\Omega_1 \cup \Omega_2$ with the pair (u_1, u_2).

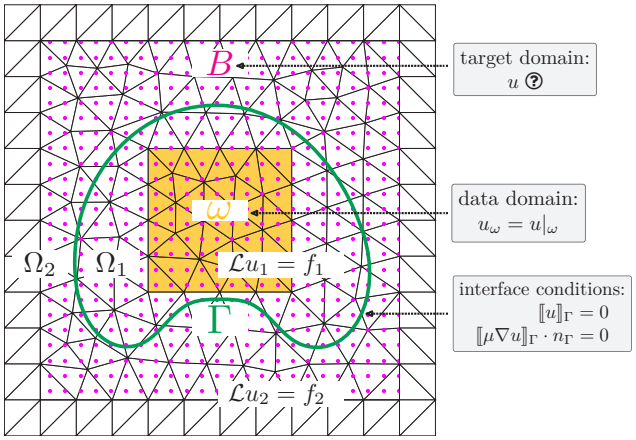

FIGURE 1.1. Sketch of geometry and data for unique continuation over an interface.

We consider the elliptic interface problem

$$\mathcal{L}u = f \text{ in } \Omega_1 \cup \Omega_2, \tag{1.1}$$

$$[\![u]\!]_\Gamma = 0 \text{ on } \Gamma, \tag{1.2}$$

$$[\![\mu\nabla u]\!]_\Gamma \cdot n_\Gamma = 0 \text{ on } \Gamma, \tag{1.3}$$

with $\mathcal{L}u := -\nabla\cdot(\mu\nabla u) - \rho u$ for a quantity μ that is discontinuous across Γ and constant on each Ω_i with $\mu_i := \mu|_{\Omega_i} > 0$. Similarly, ρ is assumed to be piecewise constant such that $\rho_i := \rho|_{\Omega_i} \in \mathbb{R}$. Here we are primarily interested in the case of the Helmholtz equation for which $\rho_i = k_i^2$ for some $k_i > 0$ representing the wavenumber, but the case of diffusion-reaction equations for which $\rho_i \leqslant 0$ is covered as well. The jump over the interface Γ is defined for $v = (v_1, v_2) \in H^1(\Omega_1 \cup \Omega_2)$ by $[\![v]\!]_\Gamma := v_1 - v_2$ and analogously for vector-valued functions. We fix the unit normal vector n_Γ of Γ to point from Ω_1 into Ω_2.

Note that no boundary data on $\partial\Omega$ is assumed to be given, which renders this problem ill-posed. To recover a weak form of stability, we will assume that measurements

$$u_\omega = u|_\omega \tag{1.4}$$

of a solution of (1.1)–(1.3) in a subset $\omega \subset \Omega$ are available. More precisely, we assume that ω is compactly contained in either Ω_1 or Ω_2. The objective is then to extend the solution from ω into a larger set $B \subset \Omega$ across the interface. Possible applications where this task occurs include inverse problems in subsurface flows, seismology and biomedical applications. From [21, Theorem 1.1], see Appendix A for details, we obtain that the following conditional stability estimate of Hölder-type holds.

Corollary 1.1. *Let $\omega \subset B \subset \Omega$ such that $B \setminus \omega$ does not touch the boundary of Ω and ω is contained either in Ω_1 or Ω_2. Then there exists a $\tau \in (0,1)$ such that for all $u \in H^1(\Omega)$ we have*

$$\|u\|_B \leqslant C \left(\|u\|_\omega + \|\mathcal{L}u\|_{H^{-1}(\Omega)}\right)^\tau \left(\|u\|_\Omega + \|\mathcal{L}u\|_{H^{-1}(\Omega)}\right)^{1-\tau}. \tag{1.5}$$

Here we introduced for $M \subset \mathbb{R}^d$ and $u, v \in L^2(M)$ the notation

$$(u, v)_M := \int_M uv \, \mathrm{d}x, \qquad \|v\|_M := \sqrt{(v, v)_M}.$$

We point out that the constant C and the parameter τ in (1.5) depend on bounds of the coefficients of the operator $\mathcal{L}$ and on certain geometrical properties. The explicit form of this dependence is in general not known. What can be characterized though for the case when ω is a ball contained in B is the rate at which C and τ degenerate as the distance between B and the boundary of Ω diminishes. We refer the reader to [21, Theorem 1.1] for the details.

1.3. **Content and structure of the article**

In this article we propose a stabilized unfitted FEM for the numerical solution of (1.1)–(1.4). To cope with the fact that the problem merely enjoys conditional stability, see Corollary 1.1, we use the stabilization framework introduced in [6], which has been applied successfully to several different problems, see e.g. [8, 15, 16, 17, 19], using geometrically *fitted* discretizations. It turns out that some additional stabilization terms on the interface are necessary to allow for the use of an *unfitted* discretization.

Unfitted methods are usually based on an implicit description of the geometry, e.g. by levelset functions. Robust and accurate numerical integration on implicitly defined domains is challenging, which renders achieving high-order geometric accuracy with unfitted methods a difficult endeavor. Here, we adopt an approach developed in [31, 34, 35] based on an isoparametric mapping of the background mesh. In this framework the exact interface Γ is represented numerically by an interface Γ_h such that $\operatorname{dist}(\Gamma, \Gamma_h) \leqslant Ch^{q+1}$ holds for a parameter $q \in \mathbb{N}$ which controls the geometric accuracy and a constant $C > 0$ independent of the mesh width h. In contrast to well-posed problems, we find that the geometric error (stemming from $\Gamma \neq \Gamma_h$) exerts an additional destabilizing effect which has to be countered by a suitable regularization term, see e.g. Figure 5.3 and Figure 5.5a.

As our main result (see Theorem 4.6) we show that the following error estimate for the extension of the solution given on the data domain ω to the target domain B holds:

$$\left\| u - u_h \circ \Phi_h^{-1} \right\|_B \leqslant Ch^{\tau q} \left(\|u\|_q + h^{-q}\delta \right).$$

Here, u_h is the numerical solution in an unfitted finite element space of order $p \geqslant q \geqslant 1$ and Φ_h is a continuous and piecewise smooth transformation mapping the exact to the approximate geometry. The term δ represent a data perturbation, $\tau \in (0, 1)$ is the Hölder exponent from Corollary 1.1 and $\|u\|_q$ some Sobolev norm of the exact solution. Comparing our theoretical result with [15, 16, 17, 19], we conclude that (granted suitable stabilization is added) unfitted methods allow to solve unique continuation problems as good as their fitted counterparts. This is also corroborated by a numerical comparsion with fitted methods presented in Section 5.3.

We summarize the three main contributions of this article:

- We solve a unique continuation problem which involves an *interface*.
- We use an *unfitted* method to discretize an *ill-posed* problem and provide a fairly complete error analysis complemented by numerical experiments.
- In particular, our analysis allows arbitrary polynomial orders and includes *geometric errors* based on the technique from [31, 34, 35].

Let us also take the opportunity to mention open problems that are beyond the scope of this article:

- In reference [15] unique continuation for the constant coefficient Helmholtz equation has been considered. Under a certain convexity condition on the geometry of data and target domain

conditional stability estimates similar to Corollary 1.1 have been derived which are robust in the wavenumber, see e.g. [15, Lemma 2]. It is not clear whether such results can be established for the interface problem considered here. As a result, we cannot characterize the dependence of our final Theorem 4.6 on the geometrical configuration explicitly. However, we point out that all the results preceding Theorem 4.6 are independent of the stability properties of the continuous problem (in particilar of the geometric configuration) since Corollary 1.1 is only applied to establish the final result.

- The error estimate in Theorem 4.6 is not robust in the contrast of the coefficients μ_i and ρ_i. This stems on the one hand from the fact that the conditional stability estimate in Corollary 1.1 is not robust in the coefficients either and on the other hand from our decision not to keep track of the dependence of the constants on bounds of the coefficients in the error analysis preceding Theorem 4.6. Actually we expect that even for the pure Poisson problem (i.e. $\rho_i = 0$) it is unlikely that error estimates that are robust in the diffusion coefficients can be obtained in the ill-posed setting considered here. This is inferred from the analysis for the well-posed case performed in reference [12] which showed that achieving robustness requires to handle a certain flux related quantity over which we lack control in the ill-posed setting.

The remainder of this article is structured as follows. In Section 2 we explain how the geometry is resolved using the isoparametric mapping technique from [31, 34]. Some additional results for this technique are derived in this article which may be of independent interest. For example, we derive useful relations between derivatives on the exact and approximate interface and show how the isoparametric mapping can be combined with a Galerkin-least squares stabilization. These results could be of interest in various settings, e.g. for convection-dominated problems, fluid problems involving interfaces or coupled bulk-surface problems. In Section 3 an unfitted isoparametric FEM for the problem (1.1)–(1.4) is introduced whose numerical analysis is carried out in Section 4. Numerical experiments are presented in Section 5. We conclude in Section 6.

2. Resolving the interface by an isoparametric mapping

This section deals with the geometrical approximation of the interface. In Subsection 2.1–2.3 three different levels of geometric accuracy will be introduced. We start in Subsection 2.1 with the exact geometry, proceed in Subsection 2.2 with the simplest approximation by a piecewise linear reference configuration and finish in Subsection 2.3 with the higher-order accurate approach from [31, 34] based on an isoparametric mapping. In Subsection 2.4 and Subsection 2.5 the basic properties of this mapping are recalled and some further extensions are derived. Please note that we have outsourced the proofs of this section into Appendix B.

2.1. The exact geometry

It is very common in unfitted FEMs to assume that the interface can be described by a smooth levelset function ϕ such that $\Gamma := \{x \in \Omega \mid \phi(x) = 0\}$. The corresponding subdomains are then given by $\Omega_1 := \{\phi < 0\}$ and $\Omega_2 := \{\phi > 0\}$. We introduce operators for restricting to these subdomains as follows:

$$(R_1 u)(x) := \begin{cases} u(x) & x \in \Omega_1, \\ 0 & \text{otherwise}, \end{cases} \qquad (R_2 u)(x) := \begin{cases} u(x) & x \in \Omega_2, \\ 0 & \text{otherwise}. \end{cases} \tag{2.1}$$

Conversely, we need to be able to extend a function defined merely on a subdomain smoothly to all of Ω. To this end, we utilize that for Lipschitz domains, see [45, Theorem 5, Chapter VI], a linear and

continuous Sobolev extension operator

$$\mathcal{E}_i : W^{m,p}(\Omega_i) \to W^{m,p}(\mathbb{R}^d), \quad \text{such that } \mathcal{E}_i|_{\Omega_i} = \mathrm{id},\ i = 1, 2, \tag{2.2}$$

exists for all $m \in \mathbb{N}_0$ and $1 \leqslant p \leqslant \infty$. Here, $W^{m,p}(\Omega_i)$ are the standard Sobolev spaces which we denote by $H^m(\Omega_i)$ when $p = 2$ as usual. For $u \in W^{m,p}(\Omega_1 \cup \Omega_2)$ it is convenient to use the notation $\mathcal{E}u = (\mathcal{E}u_1, \mathcal{E}u_2)$.

Further, we will have to consider derivatives along and normal to the interface. As in the introduction let n_Γ be the unit normal vector on Γ pointing from Ω_1 into Ω_2. Based on n_Γ we define the tangential projection $P_\Gamma := I - n_\Gamma(n_\Gamma)^T$ and surface gradient $\nabla_\Gamma := P_\Gamma \nabla$.

2.2. **The piecewise linear reference geometry**

Let us first introduce a quasi-uniform and simplicial triangulation $\mathcal{T}_h$ of Ω, which is assumed to be independent of Γ. We use the notation $\lesssim$ (and $\sim$ for $\lesssim$ and $\gtrsim$) to denote that an inequality holds with a constant independent of h and how the interface intersects the triangulation $\mathcal{T}_h$. The constant may however depend on the coefficients of the differential operator $\mathcal{L}$ in (1.1). In this work we would like to focus attention on how the geometrical resolution of the interface influences the reconstruction. To eliminate other sources of geometrical errors we assume (as in the sketch given in Figure 1.1):

Assumption 1. *Let Ω and ω be polygonal domains which are exactly fitted by $\mathcal{T}_h$.*

We denote by $V_{h,p}$ the standard H^1-conforming finite element space on $\mathcal{T}_h$ based on piecewise polynomials of order p and set $V^0_{h,p} := \{v_h \in V_{h,p} \mid v_h|_{\partial\Omega} = 0\}$. Let $\hat{\phi}$ be the piecewise linear nodal interpolation of ϕ into $V_{h,1}$. Based on $\hat{\phi}$ we define the piecewise linear reference interface $\Gamma^{\mathrm{lin}} := \{x \in \Omega \mid \hat{\phi}(x) = 0\}$, respectively the subdomains $\Omega_1^{\mathrm{lin}} := \{\hat{\phi} < 0\}$ and $\Omega_2^{\mathrm{lin}} := \{\hat{\phi} > 0\}$. An illustration of some of these geometrical quantities is given in Figure 3.1. Further, the intersection of an element with Γ^{lin} is denoted by $\Gamma_T := T \cap \Gamma^{\mathrm{lin}}$. We combine all the elements cut by the interface into the set $\mathcal{T}^\Gamma := \{T \in \mathcal{T}_h \mid \Gamma_T \neq \emptyset\}$ with corresponding domain $\Omega^\Gamma := \{x \in T \mid T \in \mathcal{T}^\Gamma\}$.

We now turn our attention to the elements in the bulk. Let $T_i := T \cap \Omega_i^{\mathrm{lin}}$ denote the portion of the element in Ω_i^{lin} and define the active mesh $\mathcal{T}_h^i := \{T \in \mathcal{T}_h \mid T_i \neq \emptyset\}$ and corresponding active domain $\Omega_i^+ := \{x \in T : T \in \mathcal{T}_h^i\}$. As for the physical domains we define corresponding restriction operators which give rise to the so called Cut-FEM space:

$$(R_i^+ u)(x) := \begin{cases} u(x) & x \in \Omega_i^+, \\ 0 & \text{otherwise,} \end{cases} \qquad V_{h,p}^\Gamma := R_1^+ V_{h,p} \oplus R_2^+ V_{h,p}. \tag{2.3}$$

Elements $v_h \in V_{h,p}^\Gamma$ have the form $v_h = (v_{h,1}, v_{h,2})$ with $v_{h,i} \in R_i^+ V_{h,p}$. Note that the introduced description of the geometry is only second order accurate, i.e. $\mathrm{dist}(\Gamma, \Gamma_h) \lesssim \mathcal{O}(h^2)$, which limits the overall accuracy of derived numerical method unless some form of correction is applied, see e.g. [4, 13].

2.3. **The isoparametric mapping**

The higher-order description of the geometry from [31, 34] is based on an interpolant $\phi_h \in V_{h,q}, q \in \mathbb{N}$ of the levelset function in a higher-order finite element space. To circumvent that for $q \geqslant 2$ the geometry description given by ϕ_h is only implicit, a mapping $\Theta_h \in [V_{h,q}]^d$ is constructed based on ϕ_h and $\hat{\phi}$ which maps the piecewise linear reference geometry to a higher order accurate approximation of the exact geometry, i.e. we have

$$\hat{\phi} \approx \phi_h \circ \Theta_h \text{ and for } \Gamma_h := \Theta_h(\Gamma^{\mathrm{lin}}) \text{ it holds: } \mathrm{dist}(\Gamma, \Gamma_h) \lesssim \mathcal{O}(h^{q+1}).$$

This means that Γ_h defined as the image of the piecewise linear reference interface under the mapping Θ_h and $\Omega_{i,h} := \Theta_h(\Omega_i^{\text{lin}})$ approximate the exact interface and subdomains with order $\mathcal{O}(h^{q+1})$ and thanks to

$$\int_{\Omega_{i,h}} f \,\mathrm{d}x = \int_{\Omega_i^{\text{lin}}} f \circ \Theta_h \,|\det(D\Theta_h)|\,\mathrm{d}y \tag{2.4}$$

it suffices to compute integrals on the piecewise linear reference configuration which is well-understood, see e.g. [7, Section 5] for details. We also define $\Omega_{i,h}^+ := \Theta_h(\Omega_i^+)$ and remark that the regularity $\phi \in C^{q+2}(U)$ where U is a neighborhood of Γ is assumed to guarantee the approximation properties of the mapping Θ_h, see [34, Section 2.1].

For the analysis (not the implementation) we will need another mapping Ψ which maps the piecewise linear reference geometry back to the exact geometry, in particular $\Psi(\Gamma^{\text{lin}}) = \Gamma$ holds. The transformation Θ_h is invertible for sufficiently small h (see [34, Section 3.5]) and we can define $\Phi_h = \Psi \circ \Theta_h^{-1}$, which then fulfills $\Phi_h(\Gamma_h) = \Gamma$ and has the smoothness property $\Phi_h \in [C(\Omega)]^d \cap [C^{q+1}(\Theta_h(\mathcal{T}_h))]^d$, where $C^{q+1}(\Theta_h(\mathcal{T}_h)) := \oplus_{T\in\mathcal{T}_h} C^{q+1}(\Theta_h(T))$, see [35]. For a detailed description on how the mappings Θ_h and Ψ are constructed we refer to [34, Section 3]. Here, we only recall the fact that both mappings are small perturbations of the identity whose action is localized in the vicinity of the interface. In particular, as ω is compactly contained in one of the subdomains it follows that for sufficiently small h it holds

$$\Phi_h|_\omega = \mathrm{id}. \tag{2.5}$$

Let us close this subsection by defining some geometrical quantities on the discrete interface Γ_h. Let n_{Γ_h} denote the unit normal vector on Γ_h. We also define the discrete tangential projection $P_{\Gamma_h} := I - n_{\Gamma_h}(n_{\Gamma_h})^T$ and surface gradient $\nabla_{\Gamma_h} := P_{\Gamma_h}\nabla$.

2.4. **Basic properties of the mappings**

As noted above, the mesh transformation is essentially a small perturbation of the identity. A quantitative version of this statement has been given in [34, Lemma 5.5] which is recalled below.

Lemma 2.1. *Let $\underline{A} := D\Phi_h$. The following holds*

$$\|\Theta_h - \Psi\|_{\infty,\Omega} + h\,\|D(\Theta_h - \Psi)\|_{\infty,\Omega} \lesssim h^{q+1}, \tag{2.6}$$

$$\|\Phi_h - \mathrm{id}\|_{\infty,\Omega} + h\,\|\underline{A} - I\|_{\infty,\Omega} \lesssim h^{q+1}. \tag{2.7}$$

Here, $\|\cdot\|_{\infty,M}$ denotes the L^∞-norm on $M \subset \mathbb{R}^d$. From the proof of [34, Lemma 5.10] we also recall the following estimates:

$$\left\|\underline{A}^{-1} - I\right\|_{\infty,\Omega} \lesssim h^q, \quad \|\det(\underline{A}) - 1\|_{\infty,\Omega} \lesssim h^q, \quad \|C_{\Phi_h}\|_{\infty,\Omega} \lesssim h^q, \tag{2.8}$$

where $C_{\Phi_h} := (\underline{A}^T\underline{A})^{-1}\det(\underline{A}) - I$. Notice also that this implies $\left\|\det(A^{-1})\right\|_{\infty,\Omega} \lesssim 1$ for h sufficiently small. We will additionally require bounds for higher derivatives of Φ_h which were stated in [34, Remark 5.6] without proof.

Lemma 2.2 (Higher order bounds for Φ_h)**.** *For $l = 2, \cdots, q+1$ it holds that*

(a) $\max_{T\in\mathcal{T}_h} \left\|D^l(\Psi - \Theta_h)\right\|_{\infty,T} \lesssim h^{q+1-l}$.

(b) $\max_{T\in\mathcal{T}_h} \left\|D^l(\Phi_h - \mathrm{id})\right\|_{\infty,\Theta_h(T)} = \max_{T\in\mathcal{T}_h} \left\|D^l\Phi_h\right\|_{\infty,\Theta_h(T)} \lesssim h^{q+1-l}$.

Proof. Given in Appendix B like the other proofs of this section. ∎

In the analysis we will frequently have to transform between exact and discrete interface. To this end, it is important to understand how the respective normal vectors and associated projections are related. We recall from [34, eq. (A.20)] that the transformation Φ_h induces the relations

$$n_\Gamma \circ \Phi_h = \frac{\underline{A}^{-T} n_{\Gamma_h}}{\left\| \underline{A}^{-T} n_{\Gamma_h} \right\|_2}, \quad n_{\Gamma_h} \circ \Phi_h^{-1} = \frac{\underline{A}^{T} n_{\Gamma}}{\left\| \underline{A}^{T} n_{\Gamma} \right\|_2}. \tag{2.9}$$

Using these relations and (2.7) it is easy to show:

Lemma 2.3 (Normal and tangential projection)**.** *For h sufficiently small the following estimates hold uniformly on Γ, respectively Γ_h.*

(a) *On Γ we have*

$$\left\| \underline{A}^{T} n_\Gamma \right\|_2 \gtrsim 1 \text{ and } \left| \left\| \underline{A}^{T} n_\Gamma \right\|_2 - 1 \right| \lesssim h^q,$$

and on Γ_h:

$$\left\| \underline{A}^{-T} n_{\Gamma_h} \right\|_2 \gtrsim 1 \text{ and } \left| \left\| \underline{A}^{-T} n_{\Gamma_h} \right\|_2 - 1 \right| \lesssim h^q.$$

(b) *The perturbation of the exact normal vector is bounded by:*

$$\left\| n_\Gamma - n_{\Gamma_h} \circ \Phi_h^{-1} \right\|_2 \lesssim h^q \text{ on } \Gamma, \quad \| n_\Gamma \circ \Phi_h - n_{\Gamma_h} \|_2 \lesssim h^q \text{ on } \Gamma_h.$$

(c) *As a result, the tangential projections satisfy:*

$$\left\| P_{\Gamma_h} \circ \Phi_h^{-1} - P_\Gamma \right\|_2 \lesssim h^q, \text{ on } \Gamma, \quad \| P_\Gamma \circ \Phi_h - P_{\Gamma_h} \|_2 \lesssim h^q, \text{ on } \Gamma_h.$$

We remark that results similar to Lemma 2.3 already appear in [29, Lemma 3.3] and [36, Lemma 17].

2.5. **Geometry errors for mapped functions**

Since Φ_h maps the discrete to the exact geometry, precomposition with this map allows to pull back functions defined on the exact geometry to the discrete geometry and vice versa. The following two lemmas discuss how various norms of these functions are related.

Lemma 2.4 (norm equivalence)**.** *Let $\tilde{v} := v \circ \Phi_h$ for $v \in H^1(\Omega_i) \cap H^2(\Psi(\mathcal{T}_h^i))$. Then it holds that*

(a) $\|\tilde{v}\|_{\Omega_{i,h}} \sim \|v\|_{\Omega_i}$ *and* $\|\nabla \tilde{v}\|_{\Omega_{i,h}} \sim \|\nabla v\|_{\Omega_i}$.

(b) *For the second derivatives we have for $\nu, \mu \in \{1, \dots, d\}$:*

$$\sum_{T \in \mathcal{T}_h^i} \int_{\Theta_h(T)} |\partial_{y_\nu} \partial_{y_\mu} \tilde{v}|^2 \, \mathrm{d}y \lesssim \sum_{|\alpha| \leqslant 2} \sum_{T \in \mathcal{T}_h^i} \int_{\Psi(T)} |D_x^\alpha v|^2 \, \mathrm{d}x.$$

While the norms involving the full gradients on Γ and Γ_h are equivalent, the corresponding statement for the normal and tangential derivatives only holds up to a geometrical error proportional to h^q. In view of Lemma 2.3 this has to be expected.

Lemma 2.5 (Derivatives at the interface)**.** *Let $\tilde{v} := v \circ \Phi_h$ for $v \in H^1(\Gamma)$. Then*

(a) *We have $\|v\|_\Gamma \sim \|\tilde{v}\|_{\Gamma_h}$ and $\|\nabla v\|_\Gamma \sim \|\nabla \tilde{v}\|_{\Gamma_h}$.*

(b) *For the normal derivates:*

$$\|\nabla\tilde{v}\cdot n_{\Gamma_h}\|_{\Gamma_h} \lesssim h^q \|\nabla v\|_\Gamma + \|\nabla v\cdot n_\Gamma\|_\Gamma\,, \quad \|\nabla v\cdot n_\Gamma\|_\Gamma \lesssim h^q \|\nabla\tilde{v}\|_{\Gamma_h} + \|\nabla\tilde{v}\cdot n_{\Gamma_h}\|_{\Gamma_h}\,.$$

(c) *And for tangential derivatives:*

$$\|\nabla_{\Gamma_h}\tilde{v}\|_{\Gamma_h} \lesssim h^q \|\nabla v\|_\Gamma + \|\nabla_\Gamma v\|_\Gamma\,, \quad \|\nabla_\Gamma v\|_\Gamma \lesssim h^q \|\nabla\tilde{v}\|_{\Gamma_h} + \|\nabla_{\Gamma_h}\tilde{v}\|_{\Gamma_h}\,.$$

Finally, we will have to quantify the extent to which a function $f\circ\Phi_h^{-1}(x)$ differs from $f(x)$ when compared at the same point x. Clearly, smoothness assumptions need to be imposed on f if one wants to guarantee that the difference is small. We remark that part (a) and (b) of the following lemma have been used before in the literature, see e.g. [32, in proof of Lemma 12].

Lemma 2.6 (Pullback)**.** *Let $M\subset\Omega$ and $U,V\subset\Omega$ be open sets that are sufficiently large to contain all line segments between points in $\Phi_h^{-1}(M)$ and M, respectively between $\Phi_h(M)$ and M.*

(a) *For $f\in W^{1,\infty}(U)$ we have $\left\|f\circ\Phi_h^{-1}-f\right\|_M \lesssim h^{q+1}\sqrt{|M|}\,\|\nabla f\|_{\infty,U}$, where $|M|$ denotes the Lebesgue measure of M.*

(b) *For $f\in W^{2,\infty}(U)$ we have*

$$\left\|\nabla(f\circ\Phi_h^{-1}-f)\right\|_M \lesssim h^{q+1}\sqrt{|M|}\,\|f\|_{W^{2,\infty}(U)} + h^q\,\|\nabla f\|_M\,.$$

(c) *For $M=\Theta_h(T)$ with $T\in\mathcal{T}_h$ and $f\in W^{3,\infty}(V)$ it holds that*

$$\|f\circ\Phi_h - f\|_{H^2(M)} \lesssim h^{q-1}\sqrt{|M|}\,\|f\|_{W^{3,\infty}(V)}\,.$$

(d) *Moreover, for $f\in H^2(\Psi(T))$ we have*

$$\left\|\partial_{x_\nu}\partial_{x_\mu}(f\circ\Phi_h)\circ\Phi_h^{-1} - \partial_{x_\nu}\partial_{x_\mu}f\right\|_{\Psi(T)} \lesssim h^q\,\|f\|_{H^2(\Psi(T))} + h^{q-1}\,\|\nabla f\|_{\Psi(T)}\,.$$

3. Isoparametric unfitted FEM

In this section we introduce a stabilized FEM for the solution of (1.1)–(1.4). Based on the technique to resolve the interface discussed in Section 2 we start in Subsection 3.1 by introducing isoparametric FEM spaces. In Subsection 3.2 we define the actual discrete variational formulation, discuss stabilization terms and record some basic properties including stability and bounds on geometric errors. The final Subsection 3.3 deals with interpolation into unfitted isoparametric FEM spaces. The results in this section are independent of the stability properties of the continuous problem, in particular equation (1.5) is never used.

3.1. Isoparametric finite element spaces

Following [34] we define the following isoparametric FEM spaces: For $\clubsuit\in\{\Gamma,0\}$:

$$V_{h,\Theta}^{\clubsuit} := \{v_h\circ\Theta_h^{-1} \mid v_h\in V_{h,p}^{\clubsuit}\},\quad V_{h,\Phi}^{\clubsuit} := \{v_h\circ\Phi_h^{-1} \mid v_h\in V_{h,\Theta}^{\clubsuit}\}, \tag{3.1}$$

$$V_{h,\Psi}^{\clubsuit} := \{v_h\circ\Psi^{-1} \mid v_h\in V_{h,p}^{\clubsuit}\}. \tag{3.2}$$

Note that $V_{h,\Theta}^{\Gamma}$ is an isoparametric version of the Cut-Finite element space defined in (2.3), while $V_{h,\Theta}^{0}$ is based on a standard finite element space on the background mesh with homogeneous Dirichlet boundary conditions on $\partial\Omega$. Since the mappings Ψ and Θ_h reduce to the identity away from the interface, it follows that functions in the transformed spaces vanish on $\partial\Omega$ as well.

Let us also note that some of the tools frequently used in the analysis involving the spaces $V_{h,p}^{\clubsuit}$ easily carry over to their curved counterparts. Indeed, as $w_h \in V_{h,\Theta}^{\clubsuit}$ is of the form $w_h = v_h \circ \Theta_h^{-1}$ with $v_h \in V_{h,p}^{\clubsuit}$ and we have from [34, Lemma 3.14] the relations

$$\|\nabla w_h\|_{\Theta_h(T)} \sim \|\nabla v_h\|_T \text{ and } \|w_h\|_{\Theta_h(T)} \sim \|v_h\|_T \tag{3.3}$$

we can transfer standard inverse inequalities from v_h to w_h, e.g.

$$\|\nabla w_h\|_{\Theta_h(T)} \sim \|\nabla v_h\|_T \lesssim h^{-1} \|v_h\|_T \sim h^{-1} \|w_h\|_{\Theta_h(T)}. \tag{3.4}$$

Since $\|w_h\|_{\Theta_h(\Gamma_T)} \sim \|v_h\|_{\Gamma_T}$, we also obtain in analogy to the case with piecewise linear geometry, see [30], that

$$\|w_h\|^2_{\Theta_h(\Gamma_T)} \lesssim h^{-1} \|w_h\|^2_{\Theta_h(T)} + h^1 \|\nabla w_h\|^2_{\Theta_h(T)}. \tag{3.5}$$

We remark that (3.3) and (3.5) are valid for general $w = v \circ \Theta_h^{-1}$ with $v \in H^1(T)$.

3.2. **Stabilized method for unique continuation**

Let us start by defining the bilinear forms usually employed for the unfitted discretization of problem (1.1)–(1.3) when homogeneous Dirichlet boundary conditions on $\partial\Omega$ are given. In the bulk we define

$$a(u,v) := \sum_{i=1,2} (\mu_i \nabla u_i, \nabla v_i)_{\Omega_i} - (\rho_i u_i, v_i)_{\Omega_i}, \tag{3.6}$$

and analogously on the discrete geometry

$$a_h(u,v) := \sum_{i=1,2} (\mu_i \nabla u_i, \nabla v_i)_{\Omega_{i,h}} - (\rho_i u_i, v_i)_{\Omega_{i,h}}. \tag{3.7}$$

On the interface we define

$$N^c(u,v) := \int_\Gamma \{\!\{-\mu \nabla v\}\!\} \cdot n_\Gamma [\![u]\!] \,\mathrm{d}S, \quad \{\!\{\mu \nabla v\}\!\} \cdot n_\Gamma := \kappa_1 \mu_1 \nabla v_1 \cdot n_\Gamma + \kappa_2 \mu_2 \nabla v_2 \cdot n_\Gamma \tag{3.8}$$

for convex weights $\kappa_1 + \kappa_2 = 1$ in the numerical flux. Note that $N^c(u,v) = 0$ for the exact solution u of (1.1)–(1.3) holds. On the discrete geometry we define N_h^c analogously where the integration is now over Γ_h and the exact normal is replaced by n_{Γ_h}. We combine bulk and interface terms into

$$A(u,v) := a(u,v) + N^c(u,v), \quad A_h(u,v) := a_h(u,v) + N_h^c(u,v). \tag{3.9}$$

Notice that $N_h^c(u,v)$ is the only term on the interface remaining in a standard unfitted Nitsche formulation [30] when v is continuous across Γ.

Next we proceed to the definition of the linear forms. Let $f_i = \mathcal{L} u_i \in W^{1,\infty}(\Omega_i)$ be the exact right hand side of (1.1). In applications exact data is usually not available. We merely have access to perturbed data

$$\tilde{f}_i := f_i + \delta f_i, \quad \delta f_i \in L^2(\Omega_i).$$

For implementation, we have to extend the data $\tilde{f}_i$ given on Ω_i to $\Omega_{i,h}$. To this end, we use the Sobolev extension operator from (2.2). Hence,

$$\mathcal{E}_i \tilde{f}_i = \mathcal{E}_i f_i + \mathcal{E}_i \delta f_i := f_{i,h} + \delta f_{i,h}$$

is well defined on $\Omega_{1,h} \cup \Omega_{2,h}$. Note that

$$\|f_{i,h}\|_{W^{1,\infty}(\Omega_{i,h})} \lesssim \|f_i\|_{W^{1,\infty}(\Omega_i)}, \quad \|\delta f_{i,h}\|_{\Omega_{i,h}} \lesssim \|\delta f_i\|_{\Omega_i}$$

holds by continuity of the extension. We write $f_h := (f_{1,h}, f_{2,h})$ and the same for δf_h and $\mathcal{E}\tilde{f}$. Then we define the linear forms

$$\ell(w) := (f, w)_{\Omega_1 \cup \Omega_2}, \ \ell_h(w_h) := (f_h, w_h)_{\Omega_{1,h} \cup \Omega_{2,h}}, \ \tilde{\ell}_h(w_h) := (\mathcal{E}\tilde{f}, w_h)_{\Omega_{1,h} \cup \Omega_{2,h}}.$$

We proceed analogously for the data domain. Recall that $u_\omega := u|_\omega$ for u being the exact solution of (1.1)–(1.3). We assume perturbed data

$$\tilde{u}_\omega := u_\omega + \delta u_\omega, \quad \delta u_\omega \in L^2(\omega)$$

is given. The strength of the entire data perturbation is measured in the norm

$$\delta := \|\delta u_\omega\|_\omega + \|\delta f\|_{\Omega_1 \cup \Omega_2}. \tag{3.10}$$

To define a stable method for the unique continuation problem, we follow the approach introduced in [6]. The idea is to formulate the ill-posed problem as a discrete optimization problem consisting of a data fidelity term: $\|u_h - \tilde{u}_\omega\|_\omega$, a term to enforce the PDE constraint: $A_h(u_h, z_h) - \tilde{\ell}_h(z_h)$, where z_h represents a Lagrange multiplier, and suitable stabilization terms to guarantee unique solvability and incorporate a priori knowledge of the solution. The stabilized FEM is then obtained from the first order optimality condition. We refer the interested reader to Remark 3.1 for a more detailed derivation and proceed now directly to the discrete variational formulation defined as follows. Find $(u_h, z_h) \in V_{h,\Theta}^\Gamma \times V_{h,\Theta}^0$ such that

$$\begin{aligned} B_h[(u_h, z_h), (v_h, w_h)] &= (\tilde{u}_\omega, v_h)_\omega + \tilde{\ell}_h(w_h) + \sum_{i=1,2} \sum_{T \in \mathcal{T}_h^i} h^2 (\mathcal{E}_i \tilde{f}_i, \mathcal{L} v_{h,i})_{\Theta_h(T_i)} \\ &= (u_\omega, v_h)_\omega + \ell_h(w_h) + \sum_{i=1,2} \sum_{T \in \mathcal{T}_h^i} h^2 (f_{i,h}, \mathcal{L} v_{h,i})_{\Theta_h(T_i)} + g(v_h, w_h) \end{aligned} \tag{3.11}$$

with

$$\begin{aligned} g(v_h, w_h) &:= (\delta u_\omega, v_h)_\omega + (\delta f_h, w_h)_{\Omega_{1,h} \cup \Omega_{2,h}} + \sum_{i=1,2} \sum_{T \in \mathcal{T}_h^i} h^2 (\delta f_{i,h}, \mathcal{L} v_{h,i})_{\Theta_h(T_i)}, \\ B_h[(u_h, z_h), (v_h, w_h)] &= A_h(v_h, z_h) + s_h(u_h, v_h) + (u_h, v_h)_\omega + A_h(u_h, w_h) - s_h^*(z_h, w_h). \end{aligned} \tag{3.12}$$

We remark that as z_h is continuous across the interface, the variables $z_{h,i}$ which appear in the definition of $A_h(v_h, z_h)$ (see e.g. (3.7)) are simply the restriction of z_h to the respective subdomains. It remains to define the primal $s_h(\cdot,\cdot)$ and dual $s_h^*(\cdot,\cdot)$ stabilization terms. We commence by introducing the constituents of the former. A fairly standard component of methods based on the framework in [6] are Galerkin-least squares:

$$J_{\mathrm{GLS}}(u_h, v_h) := \sum_{i=1,2} \sum_{T \in \mathcal{T}_h^i} h^2 (\mathcal{L} u_{h,i}, \mathcal{L} v_{h,i})_{\Theta_h(T_i)}$$

and continuous interior penalty terms:

$$J_{\mathrm{CIP}}(u_h, v_h) := \sum_{i=1,2} \sum_{F \in \mathcal{F}^i} h \int_{\Theta_h(F)} \mu_i [\![\nabla u_{h,i}]\!]_{\Theta_h(F)} \cdot n [\![\nabla v_{h,i}]\!]_{\Theta_h(F)} \cdot n \, \mathrm{d}S_{\Theta_h(F)}. \tag{3.13}$$

These terms are needed to control the H^{-1}-norm of the PDE residual, see the estimate of the terms I_1 and I_2 in Lemma 4.5. Here, $\mathcal{F}^i := \{F = T_a \cap T_b \mid T_a, T_b \in \mathcal{T}_h^i, T_a \neq T_b, F \nsubseteq \partial\Omega\}$ is used to denote the facets of the active mesh not lying on $\partial\Omega$ (see Figure 3.1 for a sketch), $[\![v]\!]_F := v|_{T_a} - v|_{T_b}$ represents the jump over a facet $F = T_a \cap T_b$ and n denotes the outward pointing normal vector of T_a. We remark that it would be sufficient to carry out the integration in (3.13) merely over $\Theta_h(F \cap T_i)$, i.e. the part of the facet lying in $\Omega_{i,h}$. However, the formulation in (3.13) is more convenient for implementation as integrals over cut facets are avoided.

Next we introduce stabilization terms on the discrete interface. The first two terms are strong analogs of the classical Nitsche terms commonly found in unfitted methods for interface problems [30, 34] and

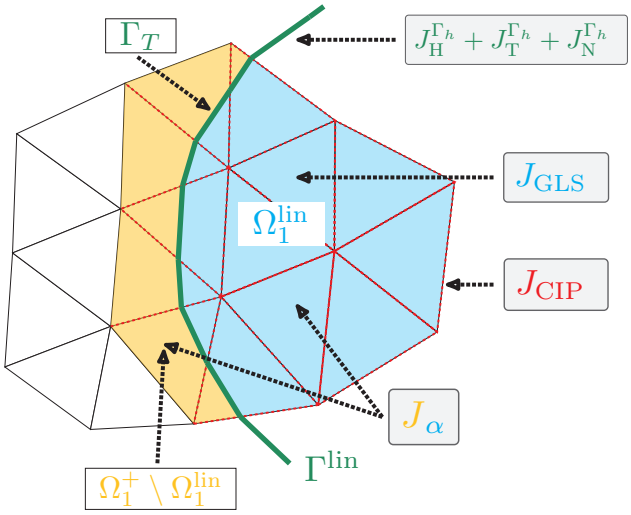

FIGURE 3.1. Domain of definition of stabilization terms on the piecewise linear reference geometry ($q = 1$). Facets in $\mathcal{F}^1$ are indicated by red dashed lines.

are required to control the terms I_3 and I_6 in Lemma 4.5. For $\bar{\mu} = (\mu_1 + \mu_2)/2$ we define

$$J_{\mathrm{H}}^{\Gamma_h}(u_h, v_h) := \frac{\bar{\mu}}{h} \int_{\Gamma_h} [\![u_h]\!]_{\Gamma_h} [\![v_h]\!]_{\Gamma_h} \mathrm{d}S_{\Gamma_h},$$
$$J_{\mathrm{N}}^{\Gamma_h}(u_h, v_h) := h \int_{\Gamma_h} [\![\mu \nabla u_h]\!]_{\Gamma_h} \cdot n_{\Gamma_h} [\![\mu \nabla v_h]\!]_{\Gamma_h} \cdot n_{\Gamma_h} \, \mathrm{d}S_{\Gamma_h}.$$

Additionally, we will stabilize the jump of the tangential gradient

$$J_{\mathrm{T}}^{\Gamma_h}(u_h, v_h) := h\bar{\mu} \int_{\Gamma_h} [\![\nabla_{\Gamma_h} u_h]\!]_{\Gamma_h} [\![\nabla_{\Gamma_h} v_h]\!]_{\Gamma_h} \mathrm{d}S_{\Gamma_h}.$$

The need for this penalty arises due to the nonconformity $V_{h,\Theta}^{\Gamma} \not\subseteq H^1(\Omega)$ as we will see later in Lemma 4.4. We combine the stabilization on the interface into

$$J^{\Gamma_h}(\cdot, \cdot) := \gamma_{\mathrm{IF}} \left(J_{\mathrm{H}}^{\Gamma_h}(\cdot, \cdot) + J_{\mathrm{N}}^{\Gamma_h}(\cdot, \cdot) + J_{\mathrm{T}}^{\Gamma_h}(\cdot, \cdot) \right), \tag{3.14}$$

where γ_{IF} is some positive parameter which we will set equal to one for the analysis. Whereas the previous terms would be consistent on the exact geometry for sufficiently smooth solutions of (1.1)–(1.3), we now introduce a weakly inconsistent Tikhonov term:

$$J_\alpha(u_h, v_h) := h^{2q} \sum_{i=1,2} \alpha_1 (u_{h,i}, v_{h,i})_{\Omega_{i,h}^+} + \alpha_2 (\nabla u_{h,i}, \nabla v_{h,i})_{\Omega_{i,h}^+}, \tag{3.15}$$

for some $\alpha_i > 0, i = 1, 2$. A weaker version of this stabilization only involving the L^2-norm has been utilized previously in the context of unique continuation problems in e.g. [8, 19]. Here we require additionally control over the gradient to compensate for geometric errors introduced by imperfect approximation of the interface, i.e. $\mathrm{dist}(\Gamma, \Gamma_h) \lesssim \mathcal{O}(h^{q+1})$. In the analysis this becomes apparent in the final estimate of the proof of Lemma 4.4 whereas we refer to Figure 5.3 for a numerical illustration. We remark that it is possible to localize these geometric errors and consequently the corresponding stabilization to a band of elements around the interface by exploiting the locality of Θ_h. As this measure did not lead to a significant improvement of the numerical results, we decided to present the technically simpler global stabilization in this paper.

We combine the introduced terms into the primal stabilization:

$$\begin{aligned} s_h(u_h, v_h) &:= \tilde{s}_h(u_h, v_h) + J_{\mathrm{GLS}}(u_h, v_h), \\ \tilde{s}_h(u_h, v_h) &:= J_{\mathrm{CIP}}(u_h, v_h) + J_\alpha(u_h, v_h) + J^{\Gamma_h}(u_h, v_h). \end{aligned} \tag{3.16}$$

The dual stabilization is simply given by

$$s_h^*(z_h, w_h) := (\mu \nabla z_h, \nabla w_h)_\Omega. \tag{3.17}$$

The dual stabilization needs to be sufficiently strong to allow for certain continuity estimates, see e.g. Lemma 3.4. Using integration by parts one could think about replacing the stabilization of the gradient by a combination of $J_{\mathrm{CIP}}(\cdot,\cdot), J_{\mathrm{GLS}}(\cdot,\cdot)$ and a penalty of the normal derivative on Γ_h and $\partial\Omega$. Note however that the presence of $J_{\mathrm{CIP}}(\cdot,\cdot)$ would introduce additional couplings in the matrix. Hence, we prefer to use the simpler choice (3.17) in this article.

Remark 3.1 (Derivation of variational formulation)**.** Let us consider the following Lagrangian:

$$\begin{aligned} L(u_h, z_h) := \frac{1}{2}\|u_h - \tilde{u}_\omega\|_\omega^2 + A_h(u_h, z_h) - \tilde{\ell}_h(z_h) + \frac{1}{2}\tilde{s}_h(u_h, u_h) \\ + \frac{1}{2}J_{\mathrm{GLS}}(u_h - \mathcal{E}u, u_h - \mathcal{E}u) - \frac{1}{2}s_h^*(z_h, z_h), \end{aligned}$$

where $\mathcal{E}u := (\mathcal{E}_1 u_1, \mathcal{E}_2 u_2)$ is a Sobolev extension of the exact solution of (1.1)–(1.3). To search for critical points of L we take the first order optimality conditions to arrive at

$$\begin{aligned} 0 &= \frac{\partial L}{\partial z_h}(w_h) = A_h(u_h, w_h) - \tilde{\ell}_h(w_h) - s_h^*(z_h, w_h), \quad \forall w_h \in V_{h,\Theta}^0, \\ 0 &= \frac{\partial L}{\partial u_h}(v_h) = (u_h - \tilde{u}_\omega, v_h)_\omega + A_h(v_h, z_h) + s_h(u_h, v_h) - J_{\mathrm{GLS}}(\mathcal{E}u, v_h), \quad \forall v_h \in V_{h,\Theta}^\Gamma. \end{aligned}$$

Adding these equations leads to the variational formulation (3.11) upon making the replacement

$$J_{\mathrm{GLS}}(\mathcal{E}u, v_h) = \sum_{i=1,2}\sum_{T\in\mathcal{T}_h^i} h^2(\mathcal{L}\mathcal{E}_i u_i, \mathcal{L}v_{h,i})_{\Theta_h(T_i)} \to \sum_{i=1,2}\sum_{T\in\mathcal{T}_h^i} h^2(\mathcal{E}_i\tilde{f}_i, \mathcal{L}v_{h,i})_{\Theta_h(T_i)}.$$

Notice that in practice the exact solution u_i is of course unknown so we cannot use $\mathcal{L}\mathcal{E}_i u_i$ directly as data. However, restricted to Ω_i we have $(\mathcal{L}\mathcal{E}_i u_i)|_{\Omega_i} = \mathcal{L}u_i = f_i$ as u_i fulfills (1.1). Hence, in the noise-free case one would replace $\mathcal{L}\mathcal{E}_i u_i$ by the data extension $\mathcal{E}_i f_i = f_{i,h}$. This will later be justified in Lemma 3.9 which shows that the corresponding consistency errors converge at optimal order. In the presence of noise we then simply replace $\mathcal{E}_i f_i$ by $\mathcal{E}_i\tilde{f}_i$, which leads to the formulation (3.11).

Remark 3.2 (Discretization space for dual variable)**.** For the unique continuation problem the dual variable z_h simply approximates[1] zero and is therefore taken from the space $V_{h,\Theta}^0$ which solely contains functions that are continuous over the interface. However, for control problems as considered in [11] the dual variable approximates the control. Following [28], the control variable of minimal L^2-norm solves the homogeneous adjoint problem which inherits the discontinuous coefficients of the original problem. Consequently, the latter then has to be discretized using a subspace of $V_{h,\Theta}^\Gamma$. We have extended our error analysis to cover this case and arrived at the same final results. Here we present the slightly simpler version using a continuous variable z_h, yet we point out that the mentioned extension could pave the way to include interfaces in the control problem considered in [11].

[1] We will quantify this statement later in Proposition 4.1.

3.2.1. *Norms*

For the error analysis we introduce the norms

$$\|v_h\|_{s_h} := s_h(v_h, v_h)^{1/2},\ v_h \in V^{\Gamma}_{h,\Theta}, \quad \|w_h\|_{s_h^*} := s_h^*(w_h, w_h)^{1/2},\ w_h \in V^0_{h,\Theta}. \tag{3.18}$$

For $\alpha_1 > 0$ it is clear that $\|\cdot\|_{s_h}$ is indeed a norm on $V^{\Gamma}_{h,\Theta}$. On the product space $V^{\Gamma}_{h,\Theta} \times V^0_{h,\Theta}$ we define the norm

$$|||(v_h, w_h)|||^2 := \|v_h\|^2_{s_h} + \|v_h\|^2_{\omega} + \|w_h\|^2_{s_h^*}. \tag{3.19}$$

Note in passing that combining Friedrich's inequality with continuity of the data extension yields

$$\begin{aligned} g(v_h, w_h) &\lesssim \|\delta u_\omega\|_\omega \|v_h\|_\omega + \|\delta f_h\|_{\Omega_{1,h}\cup\Omega_{2,h}} \|w_h\|_\Omega + J_{\mathrm{GLS}}(v_h, v_h)^{1/2}\, h\, \|\delta f_h\|_{\Omega_{1,h}\cup\Omega_{2,h}} \\ &\lesssim \delta |||(v_h, w_h)|||. \end{aligned} \tag{3.20}$$

Moreover, we will frequently make use of the common notation

$$\|v_h\|^2_{\frac{1}{2},h,\Gamma_h} := h^{-1}\|v_h\|^2_{\Gamma_h}, \qquad \|v_h\|^2_{-\frac{1}{2},h,\Gamma_h} := h\|v_h\|^2_{\Gamma_h}. \tag{3.21}$$

For measuring smoothness of the exact solution let us also define

$$\|u\|_q := \|u\|_{H^{q+1}(\Omega_1\cup\Omega_2)} + \|u\|_{W^{3,\infty}(\Omega_1\cup\Omega_2)}. \tag{3.22}$$

By Sobolev embedding theorems the second term in (3.22) involving the infinity norm can be omitted for $q \geqslant 4$ in dimensions $d \leqslant 3$.

3.2.2. *Stability, consistency and continuity*

We record some elementary properties of the introduced variational forms.

Lemma 3.3 (Consistency)**.** *Let u be a solution of* (1.1)–(1.3)*. Then*

$$A(u, v_h) = \ell(v_h), \quad \textit{for all } v_h \in V^0_{h,\Phi_h}.$$

Proof. Follows analogously to [34, Lemma 5.7]. ∎

Further note that

$$B_h[(u_h, z_h), (u_h, -z_h)] = \|u_h\|^2_{s_h} + \|u_h\|^2_{\omega} + \|z_h\|^2_{s_h^*} = |||(u_h, z_h)|||\,|||(u_h, -z_h)|||.$$

Hence,

$$\sup_{(v_h,w_h)\in V^{\Gamma}_{h,\Theta}\times V^0_{h,\Theta}} \frac{B_h[(u_h, z_h), (v_h, w_h)]}{|||(v_h, w_h)|||} \gtrsim |||(u_h, z_h)|||. \tag{3.23}$$

The bilinear form A_h is also continuous in the defined norms.

Lemma 3.4 (Continuity)**.** *For $v \in H^1(\Omega_{1,h}\cup\Omega_{2,h}) + V^{\Gamma}_{h,\Theta}$ and $w_h \in V^0_{h,\Theta}$ we have*

$$A_h(v, w_h) \lesssim \|w_h\|_{s_h^*} \left(\|\sqrt{\mu}\nabla v\|_{\Omega_{1,h}\cup\Omega_{2,h}} + \|v\|_{\Omega_{1,h}\cup\Omega_{2,h}} + \|[\![v]\!]\|_{\frac{1}{2},h,\Gamma_h} \right).$$

Proof. Using (3.5), $w_h \in V^0_{h,\Theta}$ (in particular it is univalued and smooth inside elements) and finally (3.4) we obtain[2]

$$\sum_{i=1,2}\sum_{T\in\Gamma_T} h\,\|\nabla w_{h,i}\|^2_{\Theta_h(\Gamma_T)} \lesssim \sum_{T\in\mathcal{T}_h} \left(\|\nabla w_h\|^2_{\Theta_h(T)} + h^2\,\|\nabla w_h\|^2_{H^1(\Theta_h(T))} \right) \lesssim \|w_h\|^2_{s_h^*}.$$

[2]Here, we denoted by $w_{h,i}$ the traces coming from different sides of the interface which may be different even for $w_h \in V^0_{h,\Theta}$, e.g. when the interface coincides with inter element boundaries.

Hence, the claim follows in view of

$$N_h^c(v,w_h) \lesssim \left(\sum_{i=1,2} \sum_{T\in\Gamma_T} h \left\|\nabla w_{h,i}\right\|^2_{\Theta_h(\Gamma_T)} \right)^{1/2} \left\|[\![v]\!]\right\|_{\frac{1}{2},h,\Gamma_h}. \qquad \blacksquare$$

3.2.3. *Geometry errors for bilinear and linear forms*

We recall [34, Lemma 5.10] in which the geometric errors for the standard unfitted Nitsche formulation have been analyzed.

Lemma 3.5. *For $u \in H^1(\Omega_1 \cup \Omega_2)$ and $w_h \in V^0_{h,\Theta}$ set $\tilde{u} := u \circ \Phi_h$ and $\tilde{w}_h = w_h \circ \Phi_h^{-1}$.*

(a) *The geometrical consistency error for the bilinear form in the bulk is bounded by*

$$|a(u,\tilde{w}_h) - a_h(\tilde{u},w_h)| \lesssim h^q \sum_{i=1,2} \left\|\tilde{u}_i\right\|_{H^1(\Omega_{i,h})} \left\|w_h\right\|_{H^1(\Omega)} \lesssim h^q \left\|u\right\|_{H^1(\Omega_1\cup\Omega_2)} \left\|w_h\right\|_{s_h^*}.$$

(b) *And for the linear form*

$$|\ell(\tilde{w}_h) - \ell_h(w_h)| \lesssim h^q \left\|f\right\|_{W^{1,\infty}(\Omega_1\cup\Omega_2)} \left\|w_h\right\|_{\Omega} \lesssim h^q \left\|u\right\|_{W^{3,\infty}(\Omega_1\cup\Omega_2)} \left\|w_h\right\|_{s_h^*},$$

where the second inequality assumes that u solves (1.1).

3.3. **Unfitted interpolation**

To derive error estimates in the next Section 4, we need to be able to compare the exact solution of (1.1)–(1.3) with an approximant in our unfitted curved finite element space. Since geometry data in applications often has moderate resolution, we focus here on the case of a possibly underresolved geometry. Hence, we introduce

Assumption 2. *Let $1 \leqslant q \leqslant p$.*

Under this assumption it follows thanks to [34, Theorem 3.12] that Ψ induces a family of (curved) finite elements in the sense of Bernardi [3] to which the interpolation theory developed in the latter paper can be applied. We then obtain from [3, Corollary 4.1] the existence of an interpolation operator $I_h : H^\ell(\Omega) \to V_{h,\Psi}$ with optimal approximation properties. For $v \in H^\ell(\Omega)$ it holds that

$$\left(\sum_{T\in\mathcal{T}_h} |v - I_h v|^2_{H^m(\Psi(T))} \right)^{1/2} \lesssim h^{\ell-m} \left\|v\right\|_{H^\ell(\Omega)} \tag{3.24}$$

for $0 \leqslant m \leqslant \ell \leqslant q+1$. To define an unfitted interpolation operator, we use standard techniques, see e.g. [30, 34, 41]. We define

$$I_h^\Gamma : L^2(\Omega_1\cup\Omega_2) \to V^\Gamma_{h,\Psi}, \quad I_h^\Gamma u = (R_1^+ I_h \mathcal{E}_1 R_1 u, R_2^+ I_h \mathcal{E}_2 R_2 u). \tag{3.25}$$

Sometimes we will refer to the components by $(I_h^\Gamma u)_i := R_i^+ I_h \mathcal{E}_i R_i u$. Since $(I_h^\Gamma u)_i$ will in the following only appear on domains which are part of the active mesh $\mathcal{T}_h^i$ on which the restriction R_i^+ amounts to the identity, we will drop R_i^+ from now on to ease notation. We denote by $I_h^0 : H^1_0(\Omega) \to V^0_{h,\Psi}$ the interpolation operator into the standard (curved) spaces with homogeneous Dirichlet boundary conditions on $\partial\Omega$, see [3, Theorem 5.1]. We then obtain the usual interpolation results.

Lemma 3.6 (Unfitted interpolation)**.** *Let $u \in H^\ell(\Omega_1 \cup \Omega_2)$ and $1 \leqslant m \leqslant \ell \leqslant q+1$.*

(a) *We have:*

$$\left\|(u - I_h^\Gamma u) \circ \Phi_h\right\|_{L^2(\Omega_{1,h} \cup \Omega_{2,h})} \sim \left\|u - I_h^\Gamma u\right\|_{L^2(\Omega_1 \cup \Omega_2)} \lesssim h^\ell \left\|u\right\|_{H^\ell(\Omega_1 \cup \Omega_2)}.$$

(b) *We have:*

$$\left\|\nabla(u \circ \Phi_h - I_h^\Gamma u \circ \Phi_h)\right\|_{L^2(\Omega_{1,h} \cup \Omega_{2,h})} \sim \left\|\nabla(u - I_h^\Gamma u)\right\|_{L^2(\Omega_1 \cup \Omega_2)} \lesssim h^{\ell-1} \left\|u\right\|_{H^\ell(\Omega_1 \cup \Omega_2)}.$$

(c) *For $i = 1, 2$ it holds*

$$\|(\mathcal{E}_i R_i u - I_h \mathcal{E}_i R_i u) \circ \Phi_h\|_{\frac{1}{2},h,\Gamma_h} \lesssim h^{\ell-1} \left\|u\right\|_{H^\ell(\Omega_i)}.$$

(d) *For $i = 1, 2$ and $m \geqslant 2$ it holds*

$$\|\nabla(\mathcal{E}_i R_i u - I_h \mathcal{E}_i R_i u) \circ \Phi_h\|_{-\frac{1}{2},h,\Gamma_h} \lesssim h^{\ell-1} \left\|u\right\|_{H^\ell(\Omega_i)}.$$

(e) *For $i = 1, 2$ and $m \geqslant 2$ we have*

$$\sum_{T \in \mathcal{T}_h^i} h^2 \left\|(\mathcal{E}_i R_i u - I_h \mathcal{E}_i R_i u) \circ \Phi_h\right\|^2_{H^2(\Theta_h(T))} \lesssim h^{2(\ell-1)} \left\|u\right\|^2_{H^\ell(\Omega_i)}.$$

Proof. The proofs of statements (a)–(d) are standard, see [30, 41] for the case of a piecewise linear reference geometry and [34, 35] for higher order involving the mapping. We only show statement (e), which follows by applying Lemma 2.4 and the interpolation result (3.24):

$$\begin{aligned}\sum_{T \in \mathcal{T}_h^i} h^2 \left\|(\mathcal{E}_i R_i u - I_h \mathcal{E}_i R_i u) \circ \Phi_h\right\|^2_{H^2(\Theta_h(T))} &\lesssim \sum_{T \in \mathcal{T}_h^i} h^2 \left\|\mathcal{E}_i R_i u - I_h \mathcal{E}_i R_i u\right\|^2_{H^2(\Psi_h(T))} \\ &\lesssim h^{2(\ell-1)} \left\|u\right\|^2_{H^\ell(\Omega_i)} \quad \text{for } 2 \leqslant m \leqslant \ell \leqslant q+1. \qquad \blacksquare\end{aligned}$$

As a consequence of the interpolation bounds, the continuity result of Lemma 3.4, and the geometry error estimate from Lemma 3.5 we obtain:

Lemma 3.7. *Let $u \in H^{q+1}(\Omega_1 \cup \Omega_2)$ solve (1.1)–(1.3) and $w_h \in V_{h,\Theta}^0$. Then*

$$\left|A(u, w_h \circ \Phi_h^{-1}) - A_h(I_h^\Gamma u \circ \Phi_h, w_h)\right| \lesssim h^q \left\|u\right\|_{H^{q+1}(\Omega_1 \cup \Omega_2)} \left\|w_h\right\|_{s_h^*}.$$

Proof. Since $\Phi_h(\Omega_{i,h}) = \Omega_i$ we have $(\mathcal{E}_i R_i u) \circ \Phi_h|_{\Omega_{i,h}} = (R_i u) \circ \Phi_h|_{\Omega_{i,h}}$ and similarly on Γ_h. Using this along with $N^c(u, w_h \circ \Phi_h^{-1}) = N_h^c(u \circ \Phi_h, w_h) = 0$ for u solving (1.2) yields

$$\begin{aligned}&\left|A(u, w_h \circ \Phi_h^{-1}) - A_h(I_h^\Gamma u \circ \Phi_h, w_h)\right| \\ &\qquad \leqslant \left|a(u, w_h \circ \Phi_h^{-1}) - a_h(u \circ \Phi_h, w_h)\right| + \left|A_h(\mathcal{E} u \circ \Phi_h - I_h^\Gamma u \circ \Phi_h, w_h)\right| \\ &\qquad := \mathrm{I}_1 + \mathrm{I}_2.\end{aligned}$$

By Lemma 3.5 we have $\mathrm{I}_1 \lesssim h^q \left\|u\right\|_{H^1(\Omega_1 \cup \Omega_2)} \left\|w_h\right\|_{s_h^*}$. To estimate I_2 we use continuity of $A_h(\cdot,\cdot)$, see Lemma 3.4, and the interpolation estimates from Lemma 3.6:

$$\begin{aligned}\mathrm{I}_2 &\lesssim \left\|w_h\right\|_{s_h^*} \left(\sum_{i=1,2} \|(\mathcal{E}_i R_i u - I_h \mathcal{E}_i R_i u) \circ \Phi_h)\|_{H^1(\Omega_{i,h})} + \|(\mathcal{E}_i R_i u - I_h \mathcal{E}_i R_i u) \circ \Phi_h\|_{\frac{1}{2},h,\Gamma_h} \right) \\ &\lesssim h^q \left\|w_h\right\|_{s_h^*} \left\|u\right\|_{H^{q+1}(\Omega_1 \cup \Omega_2)}. \qquad \blacksquare\end{aligned}$$

We now derive several results related to the consistency of the stabilization. By this we mean that if u solves (1.1)–(1.3), then inserting the interpolant $I_h^\Gamma u \circ \Phi_h$ into the stabilization terms should at most lead to an error of $\mathcal{O}(h^q)$. The first lemma deals with the terms on the interface.

Lemma 3.8 (Consistency of interface stabilization)**.** *Let $u \in H^{q+1}(\Omega_1 \cup \Omega_2)$ solve (1.1)–(1.3). Then*

(a) $J_{\mathrm{N}}^{\Gamma_h}\left(I_h^\Gamma u \circ \Phi_h, I_h^\Gamma u \circ \Phi_h\right)^{1/2} \lesssim h^q \left\|u\right\|_{H^{q+1}(\Omega_1\cup\Omega_2)}.$

(b) $J_{\mathrm{T}}^{\Gamma_h}\left(I_h^\Gamma u \circ \Phi_h, I_h^\Gamma u \circ \Phi_h\right)^{1/2} \lesssim h^q \left\|u\right\|_{H^{q+1}(\Omega_1\cup\Omega_2)}.$

(c) $J_{\mathrm{H}}^{\Gamma_h}\left(I_h^\Gamma u \circ \Phi_h, I_h^\Gamma u \circ \Phi_h\right)^{1/2} \lesssim h^q \left\|u\right\|_{H^{q+1}(\Omega_1\cup\Omega_2)}.$

Proof.

(a) From Lemma 2.5(b) and $[\![\mu\nabla u]\!]_\Gamma \cdot n_\Gamma = [\![\mu\nabla\mathcal{E}u]\!]_\Gamma \cdot n_\Gamma = 0$ we obtain

$$\begin{aligned}
J_{\mathrm{N}}^{\Gamma_h}\left(I_h^\Gamma u \circ \Phi_h, I_h^\Gamma u \circ \Phi_h\right) &= h\left\|[\![\mu\nabla I_h^\Gamma u \circ \Phi_h]\!]\cdot n_{\Gamma_h}\right\|_{\Gamma_h}^2 \\
&\lesssim h^{2(q+\frac12)}\sum_{i=1,2}\left\|\nabla(I_h^\Gamma u)_i\right\|_\Gamma^2 + h\left\|[\![\mu\nabla(I_h^\Gamma u - \mathcal{E}u)]\!]\cdot n_\Gamma\right\|_\Gamma^2 \\
&\lesssim h^{2(q+\frac12)}\sum_{i=1,2}\left\|\nabla(I_h^\Gamma u)_i\right\|_\Gamma^2 + h\sum_{i=1,2}\left\|\nabla(I_h^\Gamma u - \mathcal{E}u)_i\right\|_\Gamma^2 := \mathrm{I}_1 + \mathrm{I}_2.
\end{aligned}$$

From Lemma 2.5(a) and Lemma 3.6(d) we obtain

$$\mathrm{I}_2 \lesssim \sum_{i=1,2}\left\|\nabla(\mathcal{E}_i R_i u - I_h\mathcal{E}_i R_i u)\circ\Phi_h\right\|_{-\frac12,h,\Gamma_h}^2 \lesssim h^{2q}\left\|u\right\|_{H^{q+1}(\Omega_1\cup\Omega_2)}^2.$$

Similarly, $\mathrm{I}_1 \lesssim h^{2(q+\frac12)}\left\|u\right\|_{H^{q+1}(\Omega_1\cup\Omega_2)}^2$, which concludes the proof of (a).

(b) Since $u \in H^{q+1}(\Omega_1\cup\Omega_2)$ with $q \geqslant 1$ we are allowed to take the tangential derivative of equation (1.2) to obtain $[\![\nabla_\Gamma u]\!]_\Gamma = 0$. Then using Lemma 2.5(c) yields

$$\begin{aligned}
J_{\mathrm{T}}^{\Gamma_h}\left(I_h^\Gamma u \circ \Phi_h, I_h^\Gamma u \circ \Phi_h\right) &= h\bar\mu\left\|[\![\nabla_{\Gamma_h} I_h^\Gamma u \circ \Phi_h]\!]\right\|_{\Gamma_h}^2 \\
&\lesssim h^{2(q+\frac12)}\sum_{i=1,2}\left\|\nabla(I_h^\Gamma u)_i\right\|_\Gamma^2 + h\left\|[\![\nabla_\Gamma I_h^\Gamma u]\!]\right\|_\Gamma^2 \\
&\sim h^{2(q+\frac12)}\sum_{i=1,2}\left\|\nabla(I_h^\Gamma u)_i\right\|_\Gamma^2 + h\left\|[\![\nabla_\Gamma(I_h^\Gamma u - \mathcal{E}u)]\!]\right\|_\Gamma^2 \lesssim \mathrm{I}_1 + \mathrm{I}_2.
\end{aligned}$$

The terms I_1 and I_2 are the same as the ones already estimated in (a).

(c) As $\Phi_h(\Gamma_h) = \Gamma$ we have $0 = [\![u]\!]_\Gamma = [\![\mathcal{E}u]\!]_\Gamma = [\![\mathcal{E}u\circ\Phi_h]\!]_{\Gamma_h}$. This allows to skip the transformation step to the exact interface that was necessary in part (a)-(b). Hence, by applying Lemma 3.6(c):

$$\begin{aligned}
J_{\mathrm{H}}^{\Gamma_h}\left(I_h^\Gamma u \circ \Phi_h, I_h^\Gamma u \circ \Phi_h\right) &= \frac{\bar\mu}{h}\left\|[\![I_h^\Gamma u \circ \Phi_h]\!]_{\Gamma_h}\right\|_{\Gamma_h}^2 = \frac{\bar\mu}{h}\left\|[\![I_h^\Gamma u \circ \Phi_h - \mathcal{E}u\circ\Phi_h]\!]_{\Gamma_h}\right\|_{\Gamma_h}^2 \\
&\lesssim \sum_{i=1,2}\left\|(\mathcal{E}_i R_i u - I_h\mathcal{E}_i R_i u)\circ\Phi_h\right\|_{\frac12,h,\Gamma_h}^2 \lesssim h^{2q}\left\|u\right\|_{H^{q+1}(\Omega_1\cup\Omega_2)}^2. \qquad \blacksquare
\end{aligned}$$

Next we consider the least squares term.

Lemma 3.9 (Least-squares term)**.** *Let $u \in H^{q+1}(\Omega_1 \cup \Omega_2) \cap W^{3,\infty}(\Omega_1 \cup \Omega_2)$ solve (1.1)–(1.3). Then it holds that*

$$\sum_{i=1,2} \sum_{T \in \mathcal{T}_h^i} h^2 \left\| f_{i,h} - \mathcal{L}(I_h^\Gamma u \circ \Phi_h) \right\|^2_{\Theta_h(T_i)} \lesssim h^{2q} \|u\|_q^2 .$$

Proof. We have

$$\begin{aligned}
&\sum_{i=1,2} \sum_{T \in \mathcal{T}_h^i} h^2 \left\| f_{i,h} - \mathcal{L}(I_h^\Gamma u \circ \Phi_h) \right\|^2_{\Theta_h(T_i)} \\
&\quad \lesssim \sum_{i=1,2} \sum_{T \in \mathcal{T}_h^i} h^2 \|f_{i,h} - \mathcal{L}(\mathcal{E}_i u_i \circ \Phi_h)\|^2_{\Theta_h(T_i)} + \sum_{i=1,2} \sum_{T \in \mathcal{T}_h^i} h^2 \|\mathcal{L}((\mathcal{E}_i R_i u - I_h \mathcal{E}_i R_i u) \circ \Phi_h)\|^2_{\Theta_h(T)} \\
&\quad \lesssim \sum_{i=1,2} \sum_{T \in \mathcal{T}_h^i} h^2 \|f_{i,h} - \mathcal{L}(\mathcal{E}_i u_i \circ \Phi_h)\|^2_{\Theta_h(T_i)} + h^{2q} \|u\|^2_{H^{q+1}(\Omega_1 \cup \Omega_2)} ,
\end{aligned}$$

where Lemma 3.6(e) has been applied. To treat the remaining term further, we employ Lemma 2.4(a) and the triangle inequality to split

$$\begin{aligned}
&\sum_{i=1,2} \sum_{T \in \mathcal{T}_h^i} h^2 \|f_{i,h} - \mathcal{L}(\mathcal{E}_i u_i \circ \Phi_h)\|^2_{\Theta_h(T_i)} \\
&\quad \lesssim \sum_{i=1,2} \sum_{T \in \mathcal{T}_h^i} h^2 \left\| f_{i,h} \circ \Phi_h^{-1} - \mathcal{L}(\mathcal{E}_i u_i \circ \Phi_h) \circ \Phi_h^{-1} \right\|^2_{\Psi_h(T_i)} \\
&\quad \lesssim \sum_{i=1,2} \sum_{T \in \mathcal{T}_h^i} h^2 \left\| f_{i,h} \circ \Phi_h^{-1} - f_{i,h} \right\|^2_{\Psi_h(T_i)} + \sum_{i=1,2} \sum_{T \in \mathcal{T}_h^i} h^2 \left\| f_{i,h} - \mathcal{L}(\mathcal{E}_i u_i \circ \Phi_h) \circ \Phi_h^{-1} \right\|^2_{\Psi_h(T_i)} \\
&\quad := \mathrm{J}_1 + \mathrm{J}_2.
\end{aligned}$$

From Lemma 2.6(a) we obtain

$$\mathrm{J}_1 \lesssim h^{2(q+2)} \sum_{i=1,2} \|\nabla f_{i,h}\|^2_{\infty,\Omega} \lesssim h^{2(q+2)} \|f\|^2_{W^{1,\infty}(\Omega_1 \cup \Omega_2)} \lesssim h^{2(q+2)} \|u\|^2_{W^{3,\infty}(\Omega_1 \cup \Omega_2)}$$

by our smoothness assumption on the data extension. To treat J_2 we note that as $\Psi(T_i) \subset \Omega_i$ by construction it holds

$$f_{i,h}|_{\Psi(T_i)} = f_i = \mathcal{L} R_i u = (\mathcal{L}\mathcal{E}_i R_i u)|_{\Psi(T_i)}.$$

Hence, we obtain from Lemma 2.6(d)

$$\mathrm{J}_2 = \sum_{i=1,2} \sum_{T \in \mathcal{T}_h^i} h^2 \left\| \mathcal{L}(\mathcal{E}_i R_i u) - \mathcal{L}(\mathcal{E}_i u_i \circ \Phi_h) \circ \Phi_h^{-1} \right\|^2_{\Psi_h(T_i)} \lesssim h^{2q} \|u\|^2_{H^2(\Omega_1 \cup \Omega_2)} ,$$

which concludes the argument. ∎

We also have to estimate the continuous interior penalty term. The proof is similar to [32, Lemma 13] where a related estimate for a facet-based ghost penalty stabilization, which is a localized form of continuous interior penalty (possibly including higher order jumps), has been established. To this end, an interpolation operator which maps directly into $V_{h,\Theta}^\Gamma$ was constructed. Note that our interpolator I_h^Γ maps to $V_{h,\Psi}^\Gamma$ instead so that we first compose with Φ_h to obtain $I_h^\Gamma u \circ \Phi_h \in V_{h,\Theta}^\Gamma$.

Lemma 3.10 (Continuous interior penalty)**.** *Let $u \in H^{q+1}(\Omega_1 \cup \Omega_2) \cap W^{3,\infty}(\Omega_1 \cup \Omega_2)$ solve (1.1)–(1.3). Then it holds that*

$$J_{\mathrm{CIP}} \left(I_h^\Gamma u \circ \Phi_h, I_h^\Gamma u \circ \Phi_h \right)^{1/2} \lesssim h^q \|u\|_q .$$

Proof. Since $\mathcal{E}_i R_i u \in H^2(\Omega)$ we have

$$\begin{aligned} J_{\mathrm{CIP}}\left(I_h^\Gamma u\circ\Phi_h, I_h^\Gamma u\circ\Phi_h\right) &= \sum_{i=1,2}\sum_{F\in\mathcal{F}^i} h\int_{\Theta_h(F)}\mu_i\left\|[\![\nabla(\mathcal{E}_i R_i u - (I_h\mathcal{E}_i R_i u)\circ\Phi_h)]\!]_{\Theta_h(F)}\cdot n\right\|^2 \mathrm{d}S \\ &\lesssim \sum_{i=1,2}\sum_{T\in\mathcal{T}_h^i} h\left\|\nabla(\mathcal{E}_i R_i u - (I_h\mathcal{E}_i R_i u)\circ\Phi_h)\right\|^2_{\partial\Theta_h(T)} \\ &\lesssim \sum_{i=1,2}\sum_{T\in\mathcal{T}_h^i} \left\|\mathcal{E}_i R_i u - (I_h\mathcal{E}_i R_i u)\circ\Phi_h\right\|^2_{H^1(\Theta_h(T))} + h^2\left\|\mathcal{E}_i R_i u - (I_h\mathcal{E}_i R_i u)\circ\Phi_h\right\|^2_{H^2(\Theta_h(T))} \\ &:= \mathrm{I}_1 + \mathrm{I}_2. \end{aligned}$$

From Lemma 2.6(c) and Lemma 3.6(e) we obtain

$$\begin{aligned} \mathrm{I}_2 &\lesssim \sum_{i=1,2}\sum_{T\in\mathcal{T}_h^i} h^2\left\|\mathcal{E}_i R_i u - (\mathcal{E}_i R_i u)\circ\Phi_h\right\|^2_{H^2(\Theta_h(T))} + h^2\left\|(\mathcal{E}_i R_i u - I_h\mathcal{E}_i R_i u)\circ\Phi_h\right\|^2_{H^2(\Theta_h(T))} \\ &\lesssim h^{2q}\left\|u\right\|^2_{W^{3,\infty}(\Omega_1\cup\Omega_2)} + h^{2q}\left\|u\right\|^2_{H^{q+1}(\Omega_1\cup\Omega_2)}. \end{aligned}$$

The term I_1 is estimated similarly by appealing to Lemma 2.6(b) and Lemma 3.6(a)–(b). ∎

Let us define

$$\begin{aligned} S_h(I_h^\Gamma u\circ\Phi_h) := \sum_{i=1,2}\sum_{T\in\mathcal{T}_h^i} h^2\left\|f_{i,h} - \mathcal{L}(I_h^\Gamma u\circ\Phi_h)\right\|^2_{\Theta_h(T_i)} + J_\alpha\left(I_h^\Gamma u\circ\Phi_h, I_h^\Gamma u\circ\Phi_h\right) \\ + J_{\mathrm{CIP}}\left(I_h^\Gamma u\circ\Phi_h, I_h^\Gamma u\circ\Phi_h\right) + J^{\Gamma_h}\left(I_h^\Gamma u\circ\Phi_h, I_h^\Gamma u\circ\Phi_h\right) \end{aligned}$$

Then by combining the previous results we obtain:

Corollary 3.11. *Let $u \in H^{q+1}(\Omega_1\cup\Omega_2)\cap W^{3,\infty}(\Omega_1\cup\Omega_2)$ solve* (1.1)–(1.3)*. Then*

$$S_h(I_h^\Gamma u\circ\Phi_h) \lesssim h^{2q}\left\|u\right\|^2_q.$$

Proof. This follows from Lemma 3.8, Lemma 3.9, Lemma 3.10 and

$$J_\alpha\left(I_h^\Gamma u\circ\Phi_h, I_h^\Gamma u\circ\Phi_h\right) \lesssim h^{2q}\left\|u\right\|^2_{H^1(\Omega_1\cup\Omega_2)}.$$ ∎

4. **Error analysis**

Thanks to the results established in the previous two sections, the usual error analysis for methods based on the framework in [6] can be applied. First we establish convergence of the error in the stabilization norm $|||\cdot|||$, see Corollary 4.3. This result is independent of the stability properties of the continuous problem, i.e. it can be established without using equation (1.5). The stabilization norm $|||\cdot|||$ is however too weak to provide a meaningful convergence measure for practical applications. To deduce L^2-convergence in the target domain we need to utilize the conditional stability estimate (1.5). This allows us to establish Theorem 4.6, which is the only result in this article depending on the stability properties of the continuum problem.

We start by analyzing the discretization error.

Proposition 4.1. *Let $u \in H^{q+1}(\Omega_1\cup\Omega_2)\cap W^{3,\infty}(\Omega_1\cup\Omega_2)$ be the exact solution of* (1.1)–(1.4)*. Let $(u_h, z_h) \in V_{h,\Theta}^\Gamma \times V_{h,\Theta}^0$ be the solution of* (3.11)*. Then*

$$|||(u_h - I_h^\Gamma u\circ\Phi_h, z_h)||| \lesssim h^q\left\|u\right\|_q + \delta.$$

Proof. In view of the inf-sup condition (3.23), it suffices to show that

$$B_h[(u_h - I_h^\Gamma u \circ \Phi_h, z_h), (v_h, w_h)] \lesssim |||(v_h, w_h)|||(h^q \|u\|_q + \delta)$$

for all $(v_h, w_h) \in V_{h,\Theta}^\Gamma \times V_{h,\Theta}^0$. Using first order optimality (3.11) and consistency (Lemma 3.3) yields

$$\begin{aligned}
&B_h[(u_h - I_h^\Gamma u \circ \Phi_h, z_h), (v_h, w_h)] \\
&\quad = (u - I_h^\Gamma u \circ \Phi_h, v_h)_\omega + \ell_h(w_h) + g(v_h, w_h) \\
&\qquad + \sum_{i=1,2} \sum_{T \in \mathcal{T}_h^i} h^2 (f_{i,h}, \mathcal{L} v_{h,i})_{\Theta_h(T_i)} - s_h(I_h^\Gamma u \circ \Phi_h, v_h) - A_h(I_h^\Gamma u \circ \Phi_h, w_h) \\
&\quad = \underbrace{(u - I_h^\Gamma u \circ \Phi_h, v_h)_\omega}_{I_1} + \underbrace{[\ell_h(w_h) - \ell(w_h \circ \Phi_h^{-1})]}_{I_2} + \underbrace{[A(u, w_h \circ \Phi_h^{-1}) - A_h(I_h^\Gamma u \circ \Phi_h, w_h)]}_{I_3} \\
&\qquad + \underbrace{\left[\sum_{i=1,2} \sum_{T \in \mathcal{T}_h^i} h^2 (f_{i,h} - \mathcal{L} I_h^\Gamma u \circ \Phi_h, \mathcal{L} v_{h,i})_{\Theta_h(T_i)} - \tilde{s}_h(I_h^\Gamma u \circ \Phi_h, v_h) \right]}_{I_4} + \underbrace{g(v_h, w_h)}_{I_5}.
\end{aligned}$$

We consider the terms I_j separately.

- Recall that we assume $\Phi_h|_\omega = \mathrm{id}$ and $\omega \subset \Omega_i$ for exactly one $i \in \{1, 2\}$ so that from the interpolation estimates in Lemma 3.6 we obtain
$$\mathrm{I}_1 \lesssim \|v_h\|_\omega \left\| u - I_h^\Gamma u \right\|_\omega \lesssim h^{q+1} \|v_h\|_\omega \|u\|_{H^{q+1}(\Omega_1 \cup \Omega_2)}.$$
- From Lemma 3.5 and Lemma 3.7 we have
$$\mathrm{I}_2 + \mathrm{I}_3 \lesssim h^q \|u\|_q \|w_h\|_{s_h^*}.$$
- For the second to last term we apply Corollary 3.11 to obtain
$$\mathrm{I}_4 \lesssim S_h(I_h^\Gamma u \circ \Phi_h)^{1/2} \|v_h\|_{s_h} \lesssim h^q \|u\|_q \|v_h\|_{s_h}.$$
- Now only the perturbation remains which has already been estimated in (3.20).

Combining these estimates yields the claim. ∎

Remark 4.2 (Regularity assumptions on u)**.** Recall that in several of the proofs[3] of the previous section the norms $\|f\|_{W^{1,\infty}(\Omega_1 \cup \Omega_2)}$ have been replaced by the norms $\|u\|_{W^{3,\infty}(\Omega_1 \cup \Omega_2)}$ using that u solves (1.1). Note that the requirement $f \in W^{1,\infty}(\Omega_1 \cup \Omega_2)$ is already needed when performing a Strang-type error analysis of the approximation of a smooth boundary by a polygonal domain (i.e. even without the isoparametric mapping) for well-posed problems. Hence, the regularity assumptions employed here seem fairly natural.

Corollary 4.3. *Let $u \in H^{q+1}(\Omega_1 \cup \Omega_2) \cap W^{3,\infty}(\Omega_1 \cup \Omega_2)$ be the exact solution of (1.1)–(1.4). Let $(u_h, z_h) \in V_{h,\Theta}^\Gamma \times V_{h,\Theta}^0$ be the solution of (3.11). Then*

$$|||(u_h - \mathcal{E} u \circ \Phi_h, z_h)||| \lesssim h^q \|u\|_q + \delta.$$

Proof. By the triangle inequality

$$|||(u_h - \mathcal{E} u \circ \Phi_h, z_h)||| \lesssim |||(u_h - I_h^\Gamma u \circ \Phi_h, z_h)||| + |||((I_h^\Gamma u - \mathcal{E} u) \circ \Phi_h, 0)|||.$$

[3] See e.g. Lemma 3.5 (b) and Lemma 3.9. In Lemma 3.10 instead the requirement $u \in W^{3,\infty}(\Omega_1 \cup \Omega_2)$ appears to be genuine.

The first term has been estimated in Proposition 4.1 while the approximation error is easily treated by appealing to the interpolation results given in Lemma 3.6. ∎

Corollary 4.3 has to be combined with the conditional stability estimate from Corollary 1.1 to deduce convergence rates in the target domain. To this end, we would like to apply the latter to $u - u_h \circ \Phi_h^{-1}$. Unfortunately, this is not immediately possible as $u_h \circ \Phi_h^{-1} \notin H^1(\Omega)$ due to the use of an unfitted discretization. This can be fixed by adding a corrector function which removes possible jumps across the interface. The next lemma shows that the norm of this correction can be controlled by the stabilization.

Lemma 4.4. *Let $u \in H^{q+1}(\Omega_1 \cup \Omega_2) \cap W^{3,\infty}(\Omega_1 \cup \Omega_2)$ be the exact solution of (1.1)–(1.4). Let $(u_h, z_h) \in V_{h,\Theta}^{\Gamma} \times V_{h,\Theta}^{0}$ be the solution of (3.11). Let $\varphi \in H^1(\Omega_1)$ be the solution of*

$$\begin{cases} -\Delta\varphi = 0, & \text{in } \Omega_1, \\ \varphi = -[\![u_h \circ \Phi_h^{-1}]\!] & \text{on } \Gamma. \end{cases} \tag{4.1}$$

Then

$$\|\varphi\|_{H^1(\Omega_1)} \lesssim h^q \|u\|_q + \delta.$$

Proof. It follows from the Lax–Milgram lemma that

$$\|\varphi\|_{H^1(\Omega_1)} \lesssim \left\| [\![u_h \circ \Phi_h^{-1}]\!] \right\|_{H^{1/2}(\Gamma)}.$$

We have to estimate the jump term on the right hand side using convergence of $u_h - \mathcal{E}u \circ \Phi_h$ in the $|||\cdot|||$-norm, see Corollary 4.3. To achieve this, there are two main obstacles to overcome. Firstly, we have to eliminate the $H^{1/2}$-norm. To this end, we apply a Gagliardo–Nirenberg inequality on Γ and use $[\![u]\!]_\Gamma = [\![\mathcal{E}u]\!]_\Gamma = 0$ and $[\![\nabla_\Gamma u]\!]_\Gamma = [\![\nabla_\Gamma \mathcal{E}u]\!]_\Gamma = 0$ to obtain

$$\begin{aligned} \left\| [\![u_h \circ \Phi_h^{-1}]\!] \right\|_{H^{1/2}(\Gamma)}^2 &\lesssim \left\| [\![u_h \circ \Phi_h^{-1}]\!] \right\|_{L^2(\Gamma)} \left\| [\![u_h \circ \Phi_h^{-1}]\!] \right\|_{H^1(\Gamma)} \\ &\lesssim h^{-1} \left\| [\![u_h \circ \Phi_h^{-1} - \mathcal{E}u]\!] \right\|_{\Gamma}^2 + h \left\| [\![\nabla_\Gamma (u_h \circ \Phi_h^{-1} - \mathcal{E}u)]\!] \right\|_{\Gamma}^2. \end{aligned}$$

Secondly, we have to transform from the exact interface to its approximation Γ_h on which the discretization is defined. According to Lemma 2.5(c), this will lead to an additional geometrical error on the discrete interfaces involving the full gradient, that is

$$\begin{aligned} &\left\| [\![u_h \circ \Phi_h^{-1}]\!] \right\|_{H^{1/2}(\Gamma)}^2 \\ &\quad\lesssim h^{-1} \|[\![u_h - \mathcal{E}u \circ \Phi_h]\!]\|_{\Gamma_h}^2 + h \|[\![\nabla_{\Gamma_h}(u_h - \mathcal{E}u \circ \Phi_h)]\!]\|_{\Gamma_h}^2 + h^{2(q+\frac{1}{2})} \sum_{i=1,2} \|\nabla(u_{h,i} - \mathcal{E}_i u_i \circ \Phi_h)\|_{\Gamma_h}^2 \\ &\quad\lesssim |||(u_h - \mathcal{E}u \circ \Phi_h, z_h)|||^2 + h^{2(q+\frac{1}{2})} \sum_{i=1,2} (\|\nabla u_{h,i}\|_{\Gamma_h}^2 + \|\nabla \mathcal{E}_i u_i\|_{\Gamma}^2) \\ &\quad\lesssim (h^q \|u\|_q + \delta)^2 + h^{2(q+\frac{1}{2})} \sum_{i=1,2} \|\nabla u_{h,i}\|_{\Gamma_h}^2. \end{aligned}$$

Here we used that the jumps on the interface are controlled by the stabilization and Corollary 4.3. We will bound the remaining term in terms of the weak H^1-penalty using the trace[4] (3.5) and inverse inequalitites (3.4):

$$h \|\nabla u_{h,i}\|_{\Gamma_h}^2 \lesssim \sum_{T \in \mathcal{T}^\Gamma} \|u_{h,i}\|_{H^1(\Theta_h(T))}^2 + h^2 \|u_{h,i}\|_{H^2(\Theta_h(T))}^2 \lesssim \sum_{T \in \mathcal{T}^\Gamma} \|u_{h,i}\|_{H^1(\Theta_h(T))}^2.$$

[4]Here it is essential that $J_\alpha(\cdot,\cdot)$ is defined on the active mesh $\Omega_{i,h}^+$ and not merely on $\Omega_{i,h}$.

Hence,

$$h^{2(q+\frac{1}{2})}\sum_{i=1,2}\|\nabla u_{h,i}\|^2_{\Gamma_h} \lesssim J_\alpha\left(u_h,u_h\right)$$
$$\lesssim J_\alpha\left(u_h-\mathcal{E}u\circ\Phi_h,u_h-\mathcal{E}u\circ\Phi_h\right)+h^{2q}\sum_{i=1,2}\|\mathcal{E}_i u_i\circ\Phi_h\|^2_{H^1(\Omega)}$$
$$\lesssim \left(h^q\left\|u\right\|_q+\delta\right)^2$$

by Corollary 4.3. ∎

To benefit from the application of the conditional stability estimate, we have to control the terms on the right hand side of (1.5). In particular, we have to control the residual in the H^{-1}-norm, which is ensured by the following lemma.

Lemma 4.5. *Let $u\in H^{q+1}(\Omega_1\cup\Omega_2)\cap W^{3,\infty}(\Omega_1\cup\Omega_2)$ be the exact solution of (1.1)–(1.4). Let $(u_h,z_h)\in V^\Gamma_{h,\Theta}\times V^0_{h,\Theta}$ be the solution of (3.11). Then for any $w\in H^1_0(\Omega)$ it holds that*

$$a(u-u_h\circ\Phi_h^{-1},w)\lesssim\left(h^q\left\|u\right\|_q+\delta\right)\|w\|_{H^1(\Omega)}.$$

Proof. Let us define the shorthand $w_h:=w\circ\Phi_h$, $\tilde{w}_h:=w_h\circ\Phi_h^{-1}$ and $\tilde{u}=u\circ\Phi_h$. Clearly, we have to deduce the claim eventually from Corollary 4.3 for which we have to transform to the approximate geometry. Thus, the first step in this proof is to show that:

$$a(u-u_h\circ\Phi_h^{-1},w)\lesssim a_h(\tilde{u}-u_h,w_h)+\left(h^q\left\|u\right\|_q+\delta\right)\|w\|_{H^1(\Omega)} \tag{4.2}$$

holds true. To this end, note that $w=\tilde{w}_h$, so we have

$$a(u-u_h\circ\Phi_h^{-1},w)=\left[a(u,\tilde{w}_h)-a_h(\tilde{u},w_h)\right]+\left[a_h(u_h,w_h)-a(u_h\circ\Phi_h^{-1},\tilde{w}_h)\right]+a_h(\tilde{u}-u_h,w_h).$$

To estimate the first bracket we simply appeal to Lemma 3.5(a). To control the second bracket, the term $J_\alpha\left(\cdot,\cdot\right)$ is essential. By definition (3.15) of this term, Lemma 3.5(a) and Proposition 4.1 we deduce

$$\left|a_h(u_h,w_h)-a(u_h\circ\Phi_h^{-1},\tilde{w}_h)\right|\lesssim h^q\|w\|_{H^1(\Omega)}\sum_{i=1,2}\|u_{h,i}\|_{H^1(\Omega_{i,h})}$$
$$\lesssim h^q\|w\|_{H^1(\Omega)}\left(h^{-q}J_\alpha\left(u_h-I_h^\Gamma u\circ\Phi_h,u_h-I_h^\Gamma u\circ\Phi_h\right)^{1/2}+\left\|I_h^\Gamma u\circ\Phi_h\right\|_{H^1(\Omega_{1,h}\cup\Omega_{2,h})}\right)$$
$$\lesssim \|w\|_{H^1(\Omega)}\left(h^q\left\|u\right\|_q+\delta\right),$$

which shows (4.2). The next step is to bound $a_h(\tilde{u}-u_h,w_h)$ by terms which can be controlled by the stabilization. We claim that

$$a_h(\tilde{u}-u_h,w_h)\lesssim h^q\|w\|_{H^1(\Omega)}\left\|u\right\|_q+\sum_{j=1}^6\mathrm{I}_j, \tag{4.3}$$

where

$$\mathrm{I}_1:=\sum_{i=1,2}\sum_{T\in\mathcal{T}_h^i}\left(\mathcal{L}(\mathcal{E}_iR_iu\circ\Phi_h-u_{h,i}),w\circ\Phi_h-(I_h^0w)\circ\Phi_h\right)_{\Theta_h(T_i)}$$
$$\mathrm{I}_2:=\sum_{i=1,2}\sum_{F\in\mathcal{F}^i}h\int_{\Theta_h(F\cap T_i)}\mu_i[\![\nabla(\mathcal{E}_iR_iu\circ\Phi_h-u_{h,i})]\!]_{\Theta_h(F)}\cdot n\left(w\circ\Phi_h-(I_h^0w)\circ\Phi_h\right)\mathrm{d}S_{\Theta_h(F)}$$
$$\mathrm{I}_3:=N_h^c(u_h,I_h^0w\circ\Phi_h),\quad \mathrm{I}_4:=-s_h^*(z_h,I_h^0w\circ\Phi_h),\quad \mathrm{I}_5:=-(\delta f_h,I_h^0w\circ\Phi_h)_{\Omega_{1,h}\cup\Omega_{2,h}}$$
$$\mathrm{I}_6:=\left([\![\mu\nabla(\mathcal{E}u\circ\Phi_h-u_h)]\!]\cdot n_{\Gamma_h},w\circ\Phi_h-I_h^0w\circ\Phi_h\right)_{\Gamma_h}.$$

To establish (4.3), we first use consistency

$$\ell(I_h^0w)=a(u,I_h^0w),$$

which follows from Lemma 3.3. Hence,

$$a_h(\tilde{u}-u_h,w_h) = a_h(\tilde{u}-u_h, w\circ\Phi_h - I_h^0 w\circ\Phi_h) - a_h(u_h, I_h^0 w\circ\Phi_h) + [a_h(\tilde{u}, I_h^0 w\circ\Phi_h) - a(u, I_h^0 w)] + \ell(I_h^0 w). \quad (4.4)$$

By appealing to Lemma 3.5(a) we obtain

$$\left|a_h(\tilde{u}, I_h^0 w\circ\Phi_h) - a(u, I_h^0 w)\right| = \left|a(u,(I_h^0 w\circ\Phi_h)\circ\Phi_h^{-1}) - a_h(\tilde{u}, I_h^0 w\circ\Phi_h)\right| \lesssim h^q \|u\|_{H^1(\Omega_1\cup\Omega_2)} \|w\|_{H^1(\Omega)}.$$

Next we add the first order optimality condition

$$A_h(u_h, I_h^0 w\circ\Phi_h) + \mathrm{I}_4 - \ell_h(I_h^0 w\circ\Phi_h) + \mathrm{I}_5 = 0,$$

which follows from (3.11), to the right hand side of (4.4). Using that

$$\left|\ell(I_h^0 w) - \ell_h(I_h^0 w\circ\Phi_h)\right| \lesssim h^q \|u\|_q \left\|I_h^0 w\circ\Phi_h\right\|_{\Omega_{1,h}\cup\Omega_{2,h}} \lesssim h^q \|u\|_q \|w\|_{H^1(\Omega)},$$

as ensured by Lemma 3.5(b) and

$$-a_h(u_h, I_h^0 w\circ\Phi_h) + A_h(u_h, I_h^0 w\circ\Phi_h) = \mathrm{I}_3$$

yields

$$a_h(\tilde{u}-u_h,w_h) \lesssim h^q \|u\|_q \|w\|_{H^1(\Omega)} + a_h(\tilde{u}-u_h, w\circ\Phi_h - I_h^0 w\circ\Phi_h) + \mathrm{I}_3 + \mathrm{I}_4 + \mathrm{I}_5. \quad (4.5)$$

We recognize that the claimed inequality (4.3) slowly begins to appear. The final step is an element-wise integration by parts of $a_h(\tilde{u}-u_h, w\circ\Phi_h - I_h^0 w\circ\Phi_h)$, which will in particular lead to a boundary term on $\partial\Omega_{i,h}\setminus\partial\Omega$ that can be written as I_6. Hence, integration by parts yields

$$a_h(\tilde{u}-u_h, w\circ\Phi_h - I_h^0 w\circ\Phi_h) = \mathrm{I}_1 + \mathrm{I}_2 + \mathrm{I}_6.$$

Inserting this identity into (4.5) establishes (4.3).
In view of (4.2) and (4.3) it now remains to show that

$$\sum_{j=1}^{6} \mathrm{I}_j \lesssim \|w\|_{H^1(\Omega)} (h^q \|u\|_q + \delta).$$

Corollary 4.3 and interpolation estimates for I_h^0 yield

$$\mathrm{I}_1 \lesssim (J_{\mathrm{GLS}}(u_h - \mathcal{E}u\circ\Phi_h, u_h - \mathcal{E}u\circ\Phi_h))^{1/2} h^{-1} \left\|(w - I_h^0 w)\circ\Phi_h\right\|_\Omega \lesssim \|w\|_{H^1(\Omega)} (h^q \|u\|_q + \delta).$$

Similarly, by Corollary 4.3 and interpolation estimates

$$\mathrm{I}_2 \lesssim (J_{\mathrm{CIP}}(u_h - \mathcal{E}u\circ\Phi_h, u_h - \mathcal{E}u\circ\Phi_h))^{1/2} \sum_{T\in\mathcal{T}_h} h^{\frac{1}{2}} \left\|(w - I_h^0 w)\circ\Phi_h\right\|_{\partial\Theta_h(T)} \lesssim \|w\|_{H^1(\Omega)} (h^q \|u\|_q + \delta).$$

Using the estimate for $N_h^c(u_h, I_h^0 w\circ\Phi_h)$ from Lemma 3.4 along with $0 = [\![u]\!]_\Gamma = [\![\mathcal{E}u]\!]_\Gamma = [\![\mathcal{E}u\circ\Phi_h]\!]_{\Gamma_h}$ and Corollary 4.3 as well as H^1-stability of I_h^0 we obtain

$$\mathrm{I}_3 + \mathrm{I}_4 \lesssim \left\|I_h^0 w\circ\Phi_h\right\|_{s_h^*} |||(u_h - \mathcal{E}u\circ\Phi_h, z_h)||| \lesssim \|w\|_{H^1(\Omega)} (h^q \|u\|_q + \delta).$$

From Corollary 4.3 and interpolation estimates

$$\mathrm{I}_6 \lesssim (J_{\mathrm{N}}^{\Gamma_h}(u_h - \mathcal{E}u\circ\Phi_h, u_h - \mathcal{E}u\circ\Phi_h))^{1/2} \left\|(w - I_h^0 w)\circ\Phi_h\right\|_{\frac{1}{2},h,\Gamma_h} \lesssim \|w\|_{H^1(\Omega)} (h^q \|u\|_q + \delta).$$

Finally, the perturbations are bounded using continuity of the data extension and stability of the interpolation:

$$\mathrm{I}_5 \lesssim \|\delta f_h\|_{\Omega_{1,h}\cup\Omega_{2,h}} \left\|I_h^0 w\circ\Phi_h\right\|_\Omega \lesssim \delta \|w\|_{H^1(\Omega)}.$$

This concludes the argument. ∎

Finally, we can deduce convergence in the target domain. To this end, we use Corollary 1.1 which renders the resulting error estimate sensitive to the stability properties of the continuous problem.

Theorem 4.6 (L^2-error estimate in B)**.** *Let $u \in H^{q+1}(\Omega_1 \cup \Omega_2) \cap W^{3,\infty}(\Omega_1 \cup \Omega_2)$ be the exact solution of (1.1)–(1.4). Let $(u_h, z_h) \in V_{h,\Theta}^{\Gamma} \times V_{h,\Theta}^{0}$ be the solution of (3.11). Assume that $\omega \subset B \subset \Omega$ such that $B \setminus \omega$ does not touch the boundary of Ω. Then there exists a $\tau \in (0,1)$ such that*

$$\left\| u - u_h \circ \Phi_h^{-1} \right\|_B \lesssim h^{\tau q} \left(\|u\|_q + h^{-q} \delta \right).$$

Proof. As explained above, to apply the conditional stability estimate from Corollary 1.1 we first have to resolve the issue that $u_h \circ \Phi_h^{-1} \notin H^1(\Omega)$. To correct for jumps across the interface, we add the function φ as defined in (4.1) to $u_h \circ \Phi_h^{-1}$, that is

$$\bar{u}_h = (\bar{u}_{h,1}, \bar{u}_{h,2}) := (u_{h,1} \circ \Phi_h^{-1} + \varphi, u_{h,2} \circ \Phi_h^{-1}).$$

Using $\Phi_h(\Gamma_h) = \Gamma$ and that $\varphi|_\Gamma = -[\![u_h \circ \Phi_h^{-1}]\!]_\Gamma$ we obtain

$$\bar{u}_{h,2}|_\Gamma = u_{h,2}|_{\Gamma_h} = u_{h,1}|_{\Gamma_h} - [\![u_h]\!]_{\Gamma_h} = u_{h,1} \circ \Phi_h^{-1}|_\Gamma - [\![u_h \circ \Phi_h^{-1}]\!]_\Gamma = \bar{u}_{h,1}|_\Gamma.$$

It follows that $\bar{u}_h \in H^1(\Omega)$ and hence Corollary 1.1 yields

$$\begin{aligned} \left\| u - u_h \circ \Phi_h^{-1} \right\|_B &\leqslant \|u - \bar{u}_h\|_B + \|\varphi\|_{\Omega_1} \\ &\lesssim h^q \|u\|_q + \delta + \left(\|u - \bar{u}_h\|_\omega + \|\bar{r}_h\|_{H^{-1}(\Omega)} \right)^{\tau} \left(\|u - \bar{u}_h\|_\Omega + \|\bar{r}_h\|_{H^{-1}(\Omega)} \right)^{1-\tau}, \end{aligned} \quad (4.6)$$

where $\bar{r}_h := \mathcal{L}(u - \bar{u}_h)$ and Lemma 4.4 was applied to estimate $\|\varphi\|_{\Omega_1}$. We have to estimate the terms on the right hand side of (4.6).

From Lemma 4.4 and Lemma 4.5 we obtain for any $w \in H_0^1(\Omega)$ that

$$\begin{aligned} a(u - \bar{u}_h, w) &= -(\mu_1 \nabla \varphi, \nabla w)_{\Omega_1} + (\rho_1 \varphi, w)_{\Omega_1} + a(u - u_h \circ \Phi_h^{-1}, w) \\ &\lesssim \left(h^q \|u\|_q + \delta \right) \|w\|_{H^1(\Omega)}. \end{aligned}$$

Hence,

$$\|\bar{r}_h\|_{H^{-1}(\Omega)} =: \sup_{w \in H_0^1(\Omega)} \frac{a(u - \bar{u}_h, w)}{\|w\|_{H^1(\Omega)}} \lesssim h^q \|u\|_q + \delta.$$

Using the assumption $\Phi_h|_\omega = \mathrm{id}$, Corollary 4.3 and Lemma 4.4 we have

$$\|u - \bar{u}_h\|_\omega \lesssim \left\| u - u_h \circ \Phi_h^{-1} \right\|_\omega + \|\varphi\|_{\Omega_1} \sim \|u \circ \Phi_h - u_h\|_\omega + \|\varphi\|_{\Omega_1} \lesssim h^q \|u\|_q + \delta.$$

By Lemma 2.4 (a) and Lemma 4.4:

$$\|u - \bar{u}_h\|_\Omega \lesssim \left\| u - u_h \circ \Phi_h^{-1} \right\|_{\Omega_1 \cup \Omega_2} + \|\varphi\|_{\Omega_1} \lesssim \|\mathcal{E} u \circ \Phi_h - u_h\|_{\Omega_{1,h} \cup \Omega_{2,h}} + h^q \|u\|_q + \delta.$$

To control the remaining term, we use the definition of $J_\alpha(\cdot, \cdot)$ and Corollary 4.3:

$$\|\mathcal{E} u \circ \Phi_h - u_h\|_{\Omega_{1,h} \cup \Omega_{2,h}} \lesssim h^{-q} J_\alpha(\mathcal{E} u \circ \Phi_h - u_h, \mathcal{E} u \circ \Phi_h - u_h) \lesssim \|u\|_q + h^{-q} \delta.$$

Inserting these estimates into (4.6) yields the claim:

$$\begin{aligned} \left\| u - u_h \circ \Phi_h^{-1} \right\|_B &\lesssim h^q \|u\|_q + \delta + \left(h^q \left[\|u\|_q + h^{-q} \delta \right] \right)^{\tau} \left(\|u\|_q + h^{-q} \delta \right)^{1-\tau} \\ &\lesssim h^{\tau q} \left(\|u\|_q + h^{-q} \delta \right). \end{aligned}$$

■

5. Numerical experiments

We implemented the method in `ngsxfem` [33] - an Add-on which enriches the finite element library `NGSolve` [43, 44] to allow for the use of unfitted discretizations. A selection of numerical experiments

will be presented to expose strengths and weaknesses of our approach. Reproduction material for the presented experiments is avalaible at `zenodo`[5] [18] in the form of a docker image.

Throughout the experiments we use the levelset functions

$$\phi = \|x\|_\ell - 1, \qquad \|x\|_\ell := \left(\sum_{j=1}^{d} (x_j)^\ell \right)^{1/\ell}, \qquad \text{for } x \in \mathbb{R}^d, \tag{5.1}$$

for $\ell \in \{2, 4\}$ to represent the geometry. We work on a sequence of quasi-uniform simplicial meshes which are not adapted to the interface. Linear systems are solved using a sparse direct solver.

Our investigation will focus on the influence of the interface on the numerical solution of the unique continuation problem. Recall that the Hölder exponent τ and the constant C in the conditional stability estimate (1.5) depend in an unknown manner on the interface and the coefficients of the PDE. They also depend on certain convexity properties of the data and target domain as has been thoroughly investigated in reference [15] for the constant coefficient Helmholtz equation. Here we will only briefly touch on this aspect since our work is mainly devoted to the study of the material interface.

5.1. **Pure diffusion in dimension** $d = 2$

We will start with a purely diffusive problem, i.e. $\rho_i = 0, i = 1, 2$, since it is well-known that unique continuation for the Helmholtz case can be particularly challenging, see e.g. [8, 15, 19]. We consider the levelset function given in (5.1) for $\ell = 4$, where the objective is to continue the solution given in $\omega = [-0.5, 0.5]^2$ across the interface into $B = [-1.25, 1.25]^2$. A sketch of the geometrical configuration is provided in Figure 5.1b. We will consider noise-free data, i.e. $\delta = 0$ in (3.10), sampled from the exact solution

$$u = \begin{cases} \dfrac{1}{\sqrt{2}} \left(1 + \pi \dfrac{\mu_1}{\mu_2} \right) - \cos\left(\dfrac{\pi \|x\|_4^4}{4} \right) & \text{in } \Omega_1, \\ \dfrac{\mu_1 \pi}{\mu_2 \sqrt{2}} \|x\|_4 & \text{in } \Omega_2, \end{cases} \tag{5.2}$$

which is shown in Figure 5.1a as a function of $\|x\|_4$ for different levels of the contrast. Note that a kink occurs at the interface for $\mu_1 \neq \mu_2$.

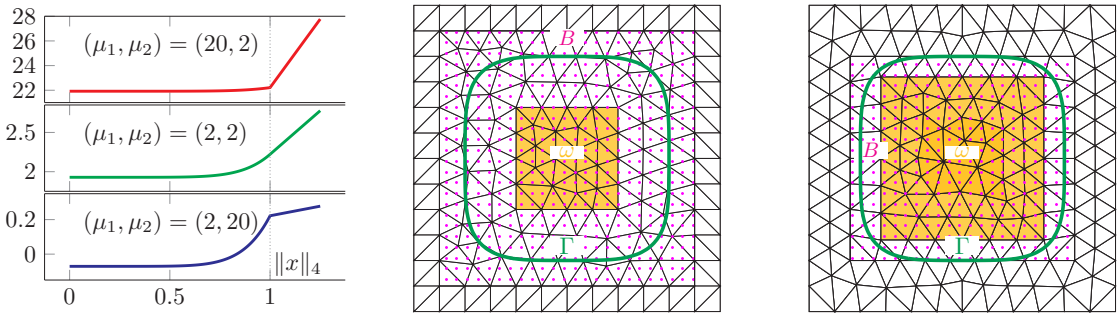

(A) Reference solution. (B) Setup: Pure diffusion. (C) Setup: Helmholtz.

FIGURE 5.1. Figure (A) shows the reference solution (5.2) in the purely diffusive case as a function of $\|x\|_4$ for different levels of the contrast. Figure (B) and (C) display a sketch of the geometrical setup for the experiments of Section 5.1, respectively 5.2.1.

The relative L^2 errors in B for different levels of the contrast are shown in Figure 5.2. Here we have set the weights in the numerical flux to $\kappa_1 = \mu_2/(\mu_1 + \mu_2)$ and $\kappa_2 = \mu_1/(\mu_1 + \mu_2)$, which is a popular

[5] `https://doi.org/10.5281/zenodo.13328144`

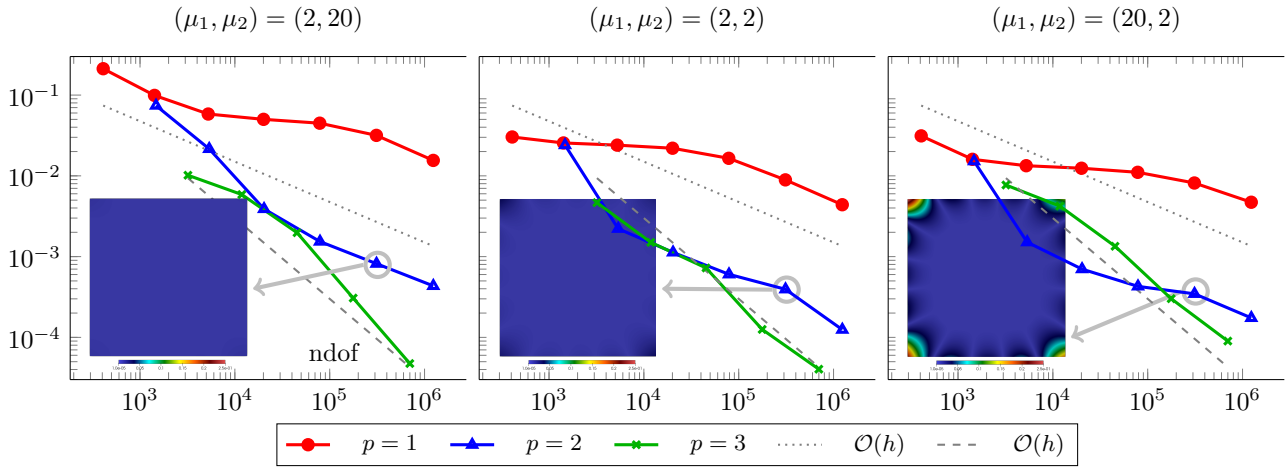

FIGURE 5.2. Dependence of the relative L^2-error in B on the contrast for a pure diffusion problem in the geometry shown in Figure 5.1b. In the insets the absolute error for the cases indicated by the arrows is shown. Here we used $q = p$. On the x-axis the number of degrees of freedom 'ndof' is displayed.

choice in the literature [20, 24, 26] for contrast problems. We observe that changing the contrast by one order of magnitude seems to have little influence on the convergence rate in the purely diffusive regime. The setup with $(\mu_1, \mu_2) = (20, 2)$ appears to be slightly more challenging than the others as the absolute error is observed to be high near the corners of the domain. Nevertheless, we still obtain reasonably accurate solutions in the target domain after a few refinement steps.

As an additional experiment let us investigate the importance of the stabilization terms. In numerical experiments it is common practice to rescale these terms by some positive constants to optimize the preasymptotic convergence behavior. The stabilization terms $J_{\text{CIP}}(\cdot,\cdot)$ and $J_{\text{GLS}}(\cdot,\cdot)$ are a standard ingredient of methods based on the framework from [6]. Parameter studies on the optimal choice of the corresponding scaling parameters can be found in the literature, see e.g. [6, 14, 19, 40]. Here, we focus on the novel terms which appeared in this work, i.e. the choice of γ_{IF} for the interface stabilization in (3.14) and the choice of α_2 in (3.15) which we introduced to counter propagation of geometric errors. The dependence of the relative L^2-error on the size of these parameters is displayed in Figure 5.3. This experiment has been carried out on the second finest mesh used for the previous convergence study. We discuss the results of the different stabilizations separately:

- The solid lines in the left plot of Figure 5.3 show that our method appears to be stable and accurate even when the stabilization on the interface is completely omitted, i.e. $\gamma_{\text{IF}} = 0$. This is in fact thanks to the presence of the Nitsche term N_h^c in the bilinear form A_h, see (3.8)–(3.9). If the latter term is omitted (dashed lines), the error increases dramatically as γ_{IF} goes to zero. Note that dropping N_h^c means to sacrifice adjoint consistency of the Nitsche formulation, which seems to be of importance here.

- If the geometry is sufficiently resolved ($q = p$) it appears that α_2 can be set to zero as well. This is reasonable since we introduced this stabilization to counter geometrical errors that are of order $\mathcal{O}(h^q)$. However, when the geometry is underresolved (central plot with $q = 1$) these geometric errors become significant and we indeed observe that the error in the target domain increases noticably when α_2 is chosen too small and $p > 1$. For $p = 1$ on the other hand, we can always set $\alpha_2 = 0$ as the discrete Poincaré inequality given in [14, Lemma 2] ensures that the gradient weighted with h is already controlled by the other stabilization terms.

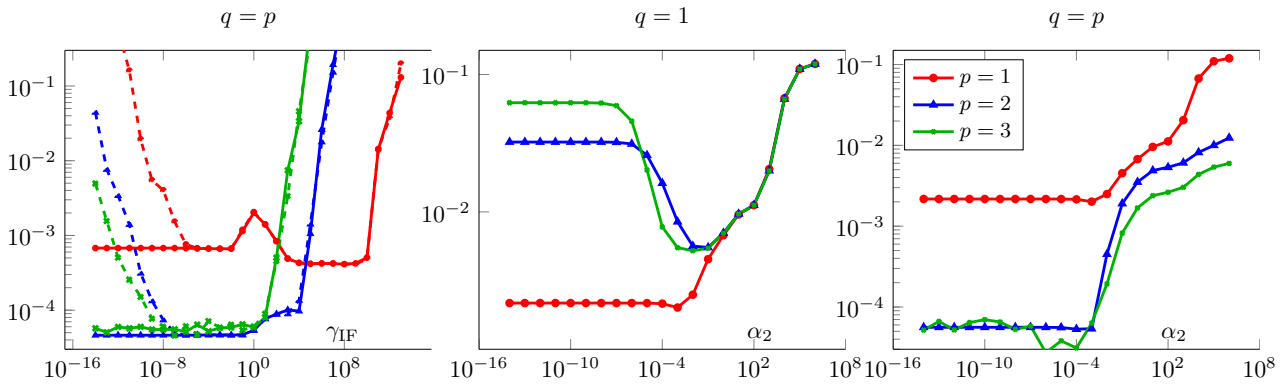

FIGURE 5.3. Dependence of the relative L^2-error in B in terms of the choice of stabilization parameters. We consider a pure diffusion problem with $(\mu_1, \mu_2) = (20, 2)$ in the geometry shown in Figure 5.1b. The solid lines in the left plot show the results for the method as defined and analyzed in this paper, while dashed lines display the results for an alternative method in which the term N_h^c in the bilinear form is omitted.

5.2. **Helmholtz problem in dimension** $d = 2$

Let us now tackle the Helmholtz problem while keeping the levelset function from Section 5.1. Here, we set $\rho_i = k_i^2$ where $k_i > 0$ is the wavenumber in the i-th subdomain and use the reference solution

$$u = \begin{cases} C_1 \cos(k_1 \|x\|_4^4) + C_2 & \text{in } \Omega_1, \\ \sin(k_2 \|x\|_4^4) & \text{in } \Omega_2, \end{cases} \tag{5.3}$$

for

$$C_1 := -\frac{k_2 \mu_2}{k_1 \mu_1} \frac{\cos(k_2)}{\sin(k_1)} \text{ and } C_2 := \sin(k_2) - C_1 \cos(k_1). \tag{5.4}$$

5.2.1. *Dependence on wavenumber and contrast ratio*

For the Helmholtz case we consider the geometrical configuration shown in Figure 5.1c. This setup is slighly less challenging than the one considered in the purely diffusive case as the data domain has been extended to $\omega = [-0.8, 0.8]^2$ whereas the target domain was reduced to $B = [-1.1, 1.1] \times [-1.0, 1.0]$. The reason for this simplification becomes immediately clear when comparing the plots of the absolute errors for the Helmholtz case shown in the insets of Figure 5.4 with the ones for the purely diffusive case given in Figure 5.2. Increasing the wavenumber k_2 in Ω_2 by a factor of six increases the error close to the boundary of the domain enormously. Whereas convergence rates of[6] $\mathcal{O}(h^{\tau(q+1)})$ with τ close to one are observed for $k_2 = 1$, the rate does not exceed second order for $k_2 = 6$. The stability is even so poor that polynomial order $p = 3$ does not perform better than order $p = 2$. Notice that the performance is equally poor for a contrast ratio of ten, i.e. for $(\mu_1, \mu_2) = (2, 20)$ as for the case of no contrast $(\mu_1, \mu_2) = (2, 2)$. The realative errors are even a bit lower in the former case, presumably because an increase of μ_2 reduces the effective wavenumber in subdomain Ω_2. In conclusion, this experiment indicates that for the considered setup the wavenumber outside the data domain is the decisive factor determining the stability of the problem.

[6] Here we use $p = q$.

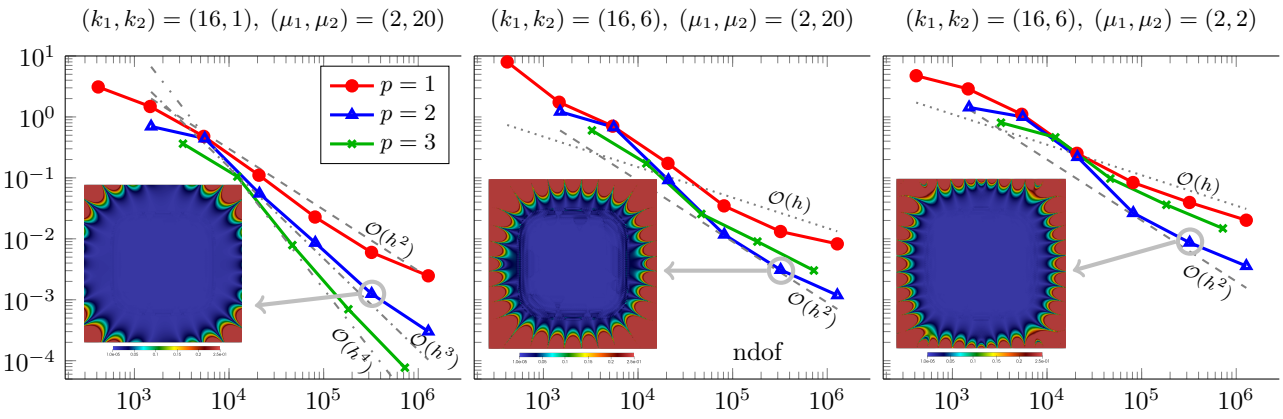

FIGURE 5.4. Dependence of the relative L^2-error in B on the coefficients for a Helmholtz problem in the geometry shown in Figure 5.1c. In the insets the absolute error for the cases indicated by the arrows is shown. Here we used $q = p$.

5.2.2. *Convex case*

As mentioned before, the stability of unique continuation problems with constant coefficients is known to be linked to the geometry of the data and target domains, see e.g. numerical experiments in [8, 15, 19]. Error estimates that are robust in the wavenumber have been proven in reference [15] when the target domain is contained in the convex hull of the data domain. We consider such a case here by setting

$$\Omega = [-1.5, 1.5]^2, \qquad B = \Omega \setminus [-1.5, 1.5] \times [1.25, 1.5], \quad \omega = B \setminus [-1.25, 1.25]^2$$

and using the same levelset function as before. The geometrical configuration and the coarsest mesh for our convergence studies are shown in Figure 5.5b. Note that we cannot expect the results from [15] to carry over directly to our setting since they apply to a problem with constant coefficients only. Here we consider the case of the Helmholtz equation with jumping coefficients and reference solution (5.3). The inset of Figure 5.6 shows a plot of this function for parameters $k_1 = 16, k_2 = 2, \mu_1 = 1, \mu_2 = 2$.

Influence of geometry approximation. In Figure 5.5a the relative L^2-errors in the target domain under mesh refinement for a poorly resolved geometry ($q = 1$) are compared with the ones based on a high-order approximation ($q = p$). For $q = 1$ the convergence for any polynomial degree p is limited by the geometrical error, i.e. $\operatorname{dist}(\Gamma, \Gamma_h) \lesssim \mathcal{O}(h^2)$, introduced by the piecewise linear approximation of the interface. Interestingly the absolute error displayed in the inset of Figure 5.5a (left) looks like a spurious resonance and a strong pollution on part of the boundary where no data is given can be observed. When increasing the resolution of the geometry to $q = p$ (central plot in Figure 5.5) these effects are reduced significantly. We observe a convergence rate of $\mathcal{O}(h^{\tau q})$ in the H^1-semi norm with τ close to one and $\mathcal{O}(h^{\tau(q+1)})$ in the L^2-norm similar as in the experiment shown in left panel of Figure 5.4. This is better than predicted by our theoretical results, which in particular do not guarantee convergence in the H^1-semi norm at all. This is because the conditional stability estimate (1.5) merely yields control of the L^2-norm in the target domain. If such an estimate giving control over the H^1-norm was available, as e.g. derived in [15, Corollary 3] for the Helmholtz equation *without interfaces* in a specific convex geometric setting, then inspection of the proof of Theorem 4.6 shows that rates of $\mathcal{O}(h^{\tau q})$ in the H^1-norm would follow.

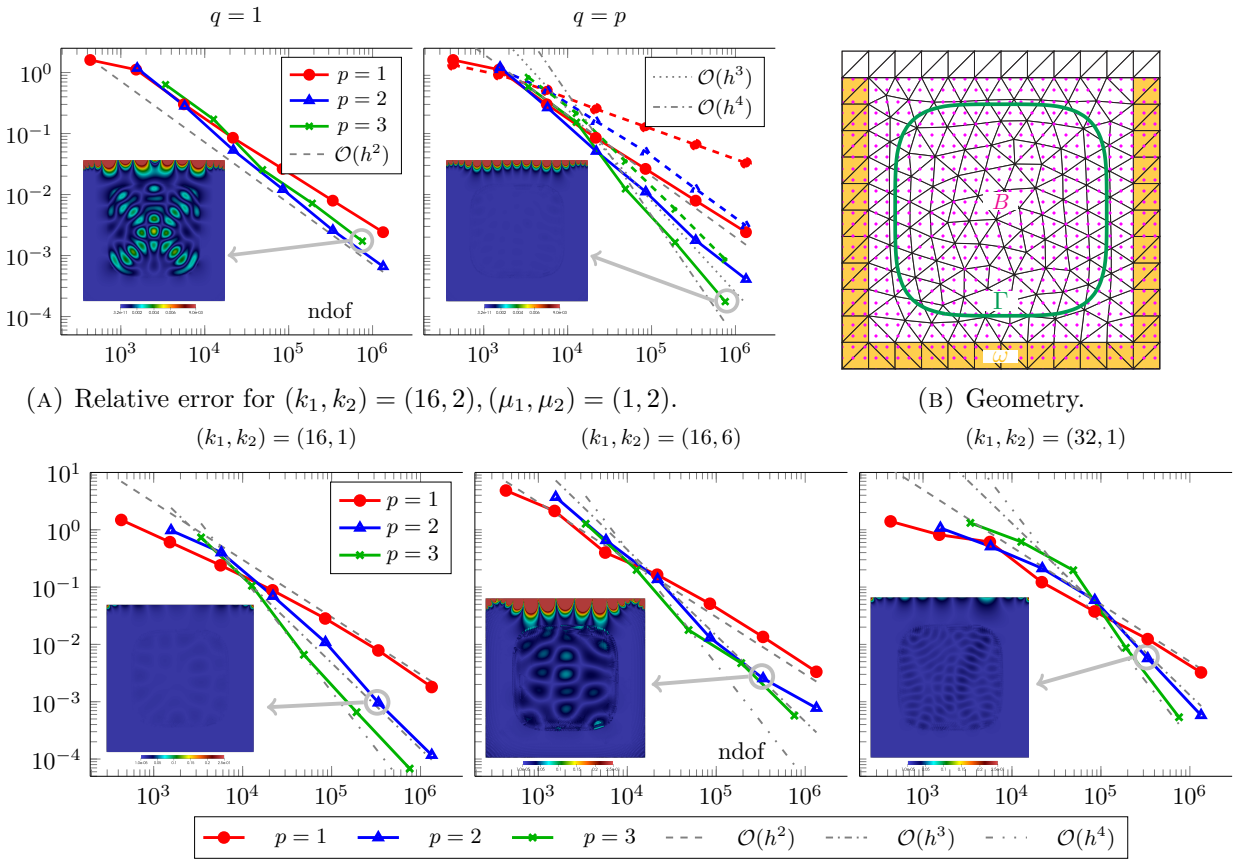

(A) Relative error for $(k_1, k_2) = (16, 2), (\mu_1, \mu_2) = (1, 2)$. (B) Geometry.

(C) Dependence of relative error on the wavenumber for $(\mu_1, \mu_2) = (2, 20)$ using $q = p$.

FIGURE 5.5. Results for a Helmholtz problem using exact data. Solid and dashed lines in (A) show the relative L^2, respectively H^1-semi error, in the target domain B. In the insets the absolute error for the cases indicated by the arrows is shown.

Influence of wavenumber. Figure 5.5c shows the effect of varying the wavenumber (k_1, k_2) while keeping (μ_1, μ_2) fixed. For $(k_1, k_2) = (16, 1)$ we observe a rate of $\mathcal{O}(h^{\tau(q+1)})$ with τ close to one. Increasing k_1 to 32 introduces a preasymptotic regime (up to about 10^5 degrees of freedom) in which a reduced rate is observed but does not change the asymptotic rate. However, increasing k_2 to 6 appears to impact the asymptotic rate negatively and leads to a large increase of the absolute error at the top of the domain. It seems that spurious modes from the top of the domain creep into the convex hull and are reflected at the interface. Even though we still observe a rate of about $\mathcal{O}(h^3)$ for $p = q = 3$ when measuring in the convex hull which is significantly better than in the central plot of Figure 5.4, where we sought to continue the solution outside the convex hull of the data, the full robustness as for the constant coefficient problem [15] is not valid. We expect that for variable coefficient problems it will be necessary to strengthen the convexity condition describing the geometry of the target domain in which robust unique continuation is possible. In particular, in the considered setting this condition has to depend on the constrast of the wavenumber.

Perturbed data. Let us now consider perturbed data of strength $\delta = \tilde{\delta}_p h^{p-\theta}$ for some $\theta \in \{0, 1, 2\}$ and with $\tilde{\delta}_p$ independent of h. In the implementation these perturbations are realized by populating the degrees of freedom of a finite element function with random noise and subsequent normalization.

Setting $q = p$ the error estimate of Theorem 4.6 predicts the following behavior:

$$\left\| u - u_h \circ \Phi_h^{-1} \right\|_B \lesssim h^{\tau p} \left(\|u\|_p + \tilde{\delta}_p h^{-\theta} \right). \tag{5.5}$$

Two different regimes can be distinguished:

- As long as $\|u\|_p h^\theta > \tilde{\delta}_p$ the first term in (5.5) will dominate. Then we expect to see the same convergence behavior as in Figure 5.5a with exact data.
- When h is small enough such that $\|u\|_p h^\theta < \tilde{\delta}_p$, then the second term takes over and the rate deteriorates to $\mathcal{O}(h^{\tau p - \theta})$.

The numerical results shown in Figure 5.6 confirm this behavior. The refinement level at which the transition from one regime to the other occurs can be shifted by scaling the coefficient $\tilde{\delta}_p$ of the noise as comparison of the solid and dashed lines in Figure 5.6 demonstrates.

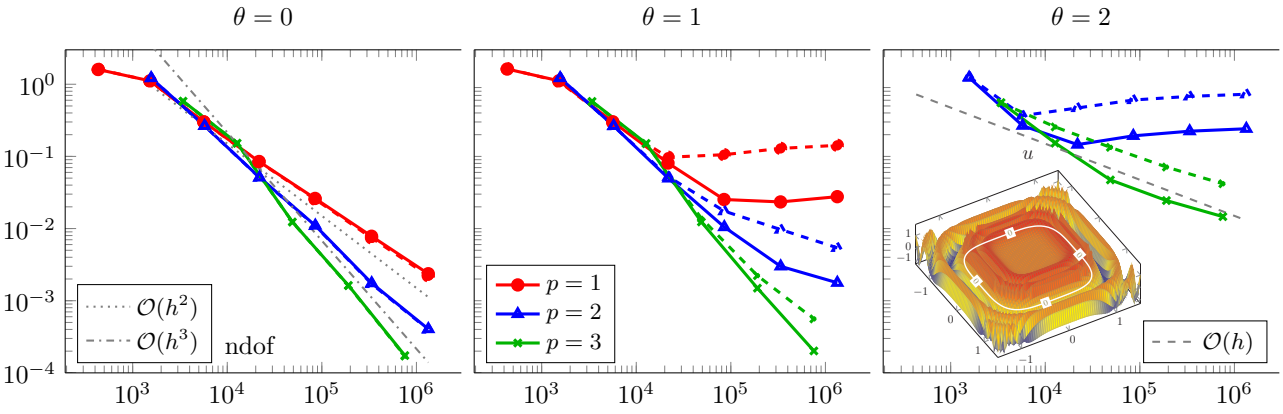

FIGURE 5.6. Results for a Helmholtz problem with $(k_1, k_2) = (16, 2), (\mu_1, \mu_2) = (1, 2)$ in the geoemetry of Figure 5.5b (B) using perturbed data with $\delta = \tilde{\delta}_p h^{p-\theta}$. Solid lines: $\tilde{\delta}_p \in [1, 8, 28]$ for $p \in [1, 2, 3]$, dashed line $\tilde{\delta}_p \in [5, 24, 80]$. All experiments use $q = p$.

5.3. **Fitted vs Unfitted methods in dimension** $d = 3$

Finally, we would like to provide a comparison between the unfitted method proposed in this work and a more traditional approach in which the mesh is fitted to the interface. The purpose of this comparison is to show that both methods yield similar results and are affected in the same way when the stability of the continuous problem deteriorates. In the fitted case we use the method from [15] which is easily generalized to allow for high-order finite elements and variable coefficients, see also [19] for an application to an elastodynamics problem.

For the geometry let us consider the unit cube $\Omega = [1.5, 1.5]^3$ with data domain $\omega = [-0.6, 0.6]^3$ and target domain $B = [-1.3, 1.3]^3$. The interface is chosen to be the unit ball, i.e. levelset function (5.1) with $\ell = 2$. A mesh which is fitted to this interface is displayed in the right inset of Figure 5.7, whereas an unfitted mesh can be seen on the left. As in the previous sections we consider the case of the Helmholtz equation and use the following reference solution

$$u = \begin{cases} (C_1 \cos(k_1 r) + C_2) \exp(-(r^2 - 1)^2) & \text{in } \Omega_1, \\ \sin(k_2 r) \exp(-(r^2 - 1)^2) & \text{in } \Omega_2, \end{cases}$$

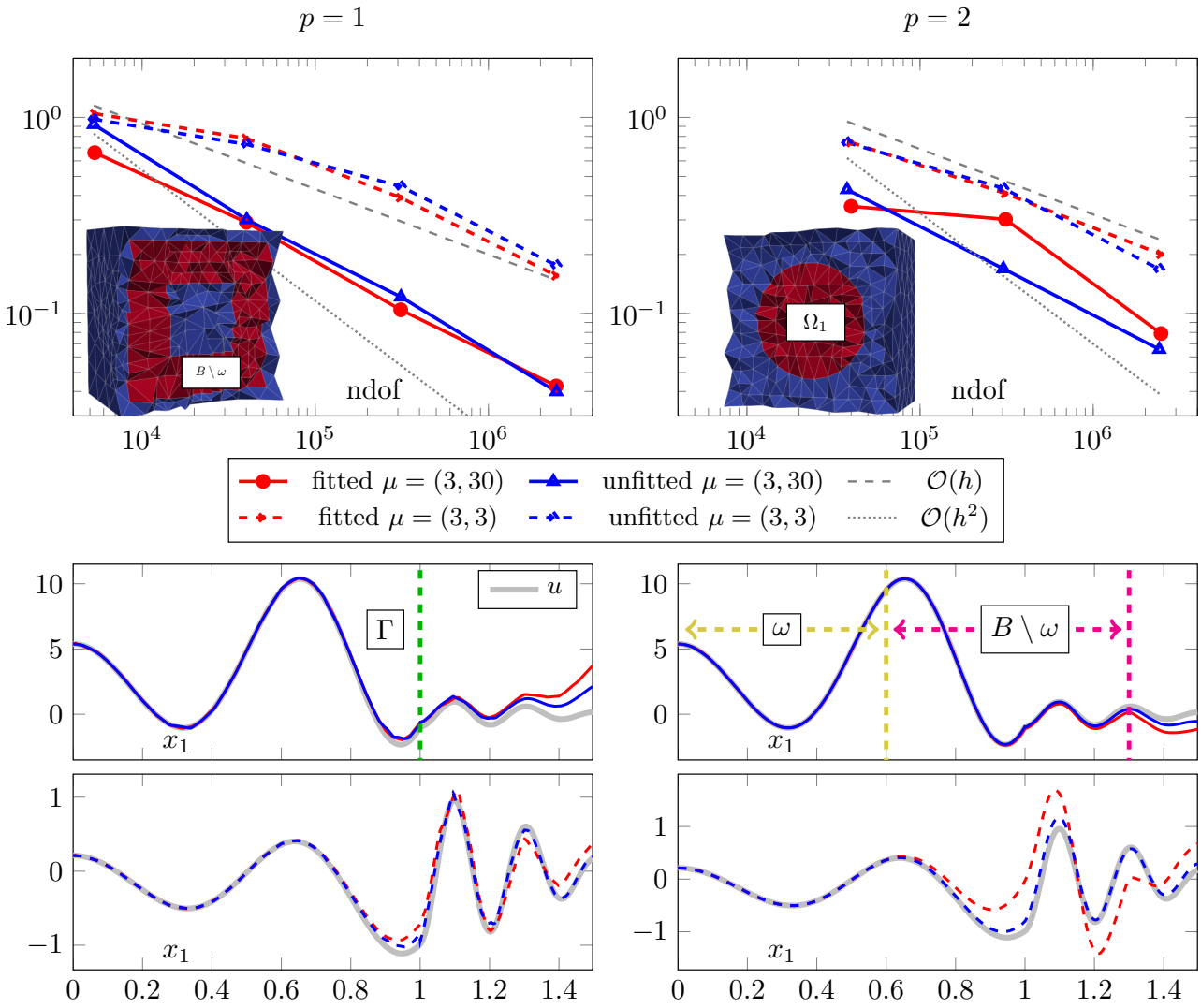

FIGURE 5.7. The upper panel compares the relative L^2 error in the target domain for the fitted and unfitted method for two different choices of (μ_1, μ_2). The lower panel shows the continuous solution and numerical approximations as a function of $(x_1, 0, 0)$ evaluated on the finest mesh considered for the respective polynomial degree. Note that the left panel presents the results for $p = 1$, whereas the right panel shows $p = 2$. We use $p = q$ for the unfitted method and accordingly employ classical curved elements of order p for the fitted method to improve the approximation of the geometry.

where $r = \|x\|_2$ and with C_1 and C_2 as in (5.4). We consider the fixed wavenumber $(k_1, k_2) = (10, 30)$ and the two cases $(\mu_1, \mu_2) = (3, 30)$ and $(\mu_1, \mu_2) = (3, 3)$. Recall from Section 5.2 that decreasing μ_2 was observed to render the problem more challenging to solve. A plot of the reference solution as a function of the first coordinate, i.e. $r = |x_1|$, is provided in the bottom panel of Figure 5.7.

The numerical results for piecewise affine and quadratic approximation are presented in the same figure. In the upper panel of the figure we can clearly see that the fitted and unfitted method (red vs. blue lines) yield very similar convergence rates. Decreasing μ_2 from 30 to 3 (solid vs. dashed lines) increases the error for both methods by the same amount. This indicates that the fitted and unfitted

approach display the same sensitivity w.r.t. deteriorating stability of the continuous problem. Hence, the unfitted method is as suited as the fitted method for solving the unique continuation problem. In fact, the qualitative approximation of the function obtained with the unfitted method can in some cases even be better than the one obtained with the fitted method as the lower panel of Figure 5.7 demonstrates.

As an outstanding issue for both approaches we mention the immense computational cost of solving the arising linear system with a direct solver, which limits the number of considered refinement levels. Actually, for the method with $p = 2$ it is not clear whether the asymptotic convergence rate has been reached yet. Iterative solution approaches are hampered by the ill-conditioning of the linear systems which reflects the ill-posed character of the corresponding continuous problems. Recently, several interesting approaches to construct efficient preconditioners [2, 25, 37] for related problems have been proposed whose suitability for our setting would be an interesting question to investigate in future work.

6. Conclusion

We have investigated an unfitted FEM for unique continuation across an interface. To establish error estimates in the unfitted setting, we had to introduce additional stabilization terms on the interface and a weak Tikhonov penalization of the gradient in the bulk. The benefit of the latter has been observed in numerical experiments featuring geometrically underresolved regimes in which the distance between Γ and Γ_h is fairly large. At the analytical level we were able to understand the need for this particular stabilization by adopting a technique introduced in [31, 34] which allows for explicit control and analysis of geometric errors. It would be interesting to investigate whether our method and its analysis could be combined with other approaches for geometry approximation and numerical integration on unfitted geometries which have been proposed in the literature. In principle, any technique that can reduce the geometric error down to the level of the discretization error in a robust[7], accurate and (desirably) efficient way should be suitable.

In numerical experiments we focused on the influence of the heterogeneity in the coefficients on our ability to extend the solution beyond the data domain. For Helmholtz problems we observed that the size of the wavenumber, particular outside the data domain, is the decisive factor that determines the stability of the problem. Contrasts in the diffusion coefficients of about one order of magnitude, on the other hand, appear to have a much smaller influence on the stability. In fact, increasing the contrast in the μ_i was even observed to be beneficial in some case, see e.g. Figure 5.7. Moreover, we observed in Section 5.2.2 that to some extent an increased stability in parts of the convex hull of the data domain appears to hold. However, the full robustness inside the convex hull as shown in [15] for the homogeneous medium does not directly carry over to the interface problem.

Appendix A. Conditional stability estimate

From [21, Theorem 1.1] we get the following result: Let $u \in H^1(\Omega)$ be a solution of (1.1) where $f \in H^{-1}(\Omega)$ is of the form

$$\langle f, v\rangle = (f_0, v)_\Omega + (F, \nabla v)_\Omega \text{ with } \|f_0\|_\Omega + \|F\|_\Omega \leqslant \varepsilon, \tag{A.1}$$

where we use the common notation $\langle\cdot,\cdot\rangle$ to denote the duality bracket on $H^{-1} \times H^1_0$. Then there exists $\bar r > 0$ such that if $0 < r_1 < r_2 < r_3 < \bar r$, $x_0 \in \Omega, \operatorname{dist}(x_0, \partial\Omega) > r_3$, there exist $C > 0, 0 < \tau < 1$ such that

$$\|u\|_{B_{r_2}(x_0)} \leqslant C \left(\|u\|_{B_{r_1}(x_0)} + \varepsilon\right)^\tau \left(\|u\|_{B_{r_3}(x_0)} + \varepsilon\right)^{1-\tau}. \tag{A.2}$$

[7] In particular, guaranteeing positiveness of quadrature weights.

Here, $B_{r_j}(x_0)$ denotes the ball around x_0 with radius $r_j, j = 1, 2, 3$. We note that any $f \in H^{-1}(\Omega)$ with $\|f\|_{H^{-1}(\Omega)} \leqslant \varepsilon/2$ can be written in the form (A.1). Indeed, let $\phi \in H_0^1(\Omega)$ be the solution of the auxiliary problem

$$-\Delta\phi + \phi = f \in H^{-1}(\Omega).$$

Then clearly,

$$\langle f, v\rangle = (\phi, v)_\Omega + (\nabla\phi, \nabla v)_\Omega$$

for all $v \in H_0^1(\Omega)$. So we can take $f_0 = \phi$ and $F = \nabla\phi$. Further,

$$\|f\|_{H^{-1}(\Omega)} = \sup_{v:\|v\|_{H^1(\Omega)=1}} \langle f, v\rangle = \sup_{v:\|v\|_{H^1(\Omega)=1}} (\phi, v)_\Omega + (\nabla\phi, \nabla v)_\Omega = \|\phi\|_{H^1(\Omega)}.$$

Hence,

$$\|f_0\|_\Omega + \|F\|_\Omega \leqslant 2\|\phi\|_{H^1(\Omega)} = 2\|f\|_{H^{-1}(\Omega)} \leqslant \varepsilon.$$

Thus (A.2) yields

$$\|u\|_{B_{r_2}(x_0)} \leqslant C\left(\|u\|_{B_{r_1}(x_0)} + \|\mathcal{L}u\|_{H^{-1}(\Omega)}\right)^\tau \left(\|u\|_{B_{r_3}(x_0)} + \|\mathcal{L}u\|_{H^{-1}(\Omega)}\right)^{1-\tau}.$$

The general case for $\omega \subset B \subset \Omega$ such that $B \setminus \omega$ does not touch the boundary stated in Corollary 1.1 then follows by using a covering argument, see [1, Section 5] or also [42]. In this argument one essentially reaches a point in the target domain B by using a sequence of balls. If the point in question happens to be contained in the convex hull of the data domain, then several paths to reach it are possible which have similar stability properties. On the other hand, for a point outside the convex hull only one path with the best stability properties exists.

Appendix B. Proofs involving the isoparametric mapping

Proof of Lemma 2.2.

(a) From the construction of the mesh transformation, see [34, Section 3], we recall that

$$\Psi - \Theta_h = \begin{cases} \Psi^\Gamma - \Theta_h^\Gamma & \text{on } \Omega^\Gamma, \\ E^{\partial\Omega^\Gamma}(\Psi^\Gamma - \Theta_h^\Gamma) & \text{on } \Omega_+^\Gamma \setminus \Omega^\Gamma, \\ 0 & \text{on } \Omega \setminus \Omega_+^\Gamma. \end{cases}$$

Here, Ψ^Γ and Θ_h^Γ are local mappings on the cut elements Ω^Γ which are extended to a slightly larger domain Ω_+^Γ by a certain extension operator $E^{\partial\Omega^\Gamma}$, which according to [34, Theorem 3.11] fulfills

$$\max_{T\in\mathcal{T}_+^\Gamma\setminus\mathcal{T}^\Gamma} \left\|D^n E^{\partial\Omega^\Gamma} w\right\|_{\infty,T} \lesssim \max_{F\in\mathcal{F}(\partial\Omega^\Gamma)} \sum_{r=n}^{q+1} h^{r-n} \|D^r w\|_{\infty,F}, \quad n = 2, \dots, q+1. \tag{B.1}$$

Here, $\mathcal{F}(\partial\Omega^\Gamma)$ denotes the set of all edges ($d = 2$) or faces ($d = 3$) in $\partial\Omega^\Gamma$ and $\mathcal{T}_+^\Gamma \setminus \mathcal{T}^\Gamma$ the set of elements convering the extended region $\Omega_+^\Gamma \setminus \Omega^\Gamma$. We also have from [34, Lemma 3.7] the estimate

$$\sum_{r=0}^{q+1} h^r \max_{T\in\mathcal{T}^\Gamma} \left\|D^r(\Psi^\Gamma - \Theta_h^\Gamma)\right\|_{\infty,T} \lesssim h^{q+1} \tag{B.2}$$

which already proves the claim (a) on Ω^Γ. It remains to consider

$$\max_{T\in\mathcal{T}_+^\Gamma\setminus\mathcal{T}^\Gamma}\left\|D^l E^{\partial\Omega^\Gamma}(\Psi^\Gamma-\Theta_h^\Gamma)\right\| \lesssim \max_{F\in\mathcal{F}(\partial\Omega^\Gamma)}\sum_{r=l}^{q+1} h^{r-l}\left\|D^r(\Psi^\Gamma-\Theta_h^\Gamma)\right\|_{\infty,F}$$
$$\lesssim h^{-l}\max_{T\in\mathcal{T}^\Gamma}\sum_{r=0}^{q+1} h^r\left\|D^r(\Psi^\Gamma-\Theta_h^\Gamma)\right\|_{\infty,T}\lesssim h^{q+1-l}.$$

where (B.1) and (B.2) have been employed. For passing from the facet to the element we also used that the involved functions are continuous on the elements so that the L^∞-norm coincides with the supremum norm, see e.g. [27, Chapter 6.1].

(b) Recall that $\Phi-\mathrm{id}=(\Psi-\Theta_h)\Theta_h^{-1}$. In [32, Lemma 2] the bounds

$$\left\|D^l\Theta_h^{-1}\right\|_{\infty,\Theta_h(T)}\lesssim 1,\qquad \text{for } l\in\{1,\dots,q+1\}$$

have been shown (for $l\in\{0,1\}$ the bounds actually hold globally, see proof of [34, Lemma 5.5.]). Hence, in view of part (a) the claim follows from the product rule. ∎

Proof of Lemma 2.3. We will only prove the results on Γ as the statements on Γ_h follow analogously.

(a) From the reverse triangle inequality we obtain for $x\in\Gamma$

$$\left|\left\|\underline{A}^T(x)n_\Gamma(x)\right\|_2-1\right|=\left|\left\|\underline{A}^T(x)n_\Gamma(x)\right\|_2-\|n_\Gamma(x)\|_2\right|\leqslant\left\|(\underline{A}^T(x)-I)n_\Gamma(x)\right\|_2.$$

Since $\Theta_h(\mathcal{T}_h)$ covers Ω, there exists an element T such that $x\in\Theta_h(T)$. As $\underline{A}^T$ is continuous on $\Theta_h(T)$ we obtain:

$$\left\|(\underline{A}^T(x)-I)n_\Gamma(x)\right\|_2\lesssim\left\|\underline{A}^T-I\right\|_{\infty,\Theta_h(T)}\lesssim h^q,$$

where (2.7) was used in the last step. As a result, the lower bound

$$\left\|\underline{A}^T n_\Gamma\right\|_2\geqslant 1-\left|\left\|\underline{A}^T n_\Gamma\right\|_2-1\right|\gtrsim 1$$

for h sufficiently small follows.

(b) Using (2.9), (2.7) and (a) we obtain

$$\left\|n_\Gamma-n_{\Gamma_h}\circ\Phi_h^{-1}\right\|_2=\frac{1}{\left\|\underline{A}^T n_\Gamma\right\|_2}\left\|n_\Gamma\left\|\underline{A}^T n_\Gamma\right\|-\underline{A}^T n_\Gamma\right\|_2$$
$$\lesssim\left\|n_\Gamma\left(\left\|\underline{A}^T n_\Gamma\right\|_2-1\right)+\left(I-\underline{A}^T\right)n_\Gamma\right\|_2\lesssim\left|\left\|\underline{A}^T n_\Gamma\right\|_2-1\right|+\left\|I-\underline{A}^T\right\|_2\lesssim h^q.$$

(c) From the result established in (b) we obtain

$$\left\|P_{\Gamma_h}\circ\Phi_h^{-1}-P_\Gamma\right\|_2=\left\|(n_{\Gamma_h}\circ\Phi_h^{-1}-n_\Gamma)(n_{\Gamma_h}\circ\Phi_h^{-1})^T+n_\Gamma(n_{\Gamma_h}\circ\Phi_h^{-1}-n_\Gamma)^T\right\|_2$$
$$\lesssim\left\|n_{\Gamma_h}\circ\Phi_h^{-1}-n_\Gamma\right\|_2+\left\|(n_{\Gamma_h}\circ\Phi_h^{-1}-n_\Gamma)^T\right\|_2\lesssim h^q.$$ ∎

Proof of Lemma 2.4.

(a) See [34, proof of Lemma 5.10].

(b) According to the chain rule

$$\partial_{y_\nu}\partial_{y_\mu}\tilde{v}(y)=\sum_{j=1}^d\sum_{k=1}^d(\partial_j\partial_k v)\circ\Phi_h(y)\partial_{y_\nu}[\Phi_h]_j(y)\partial_{y_\mu}[\Phi_h]_k(y)+\sum_{k=1}^d(\partial_k v)\circ\Phi_h(y)\partial_{y_\nu}\partial_{y_\mu}[\Phi_h]_k(y),$$

where $[\Phi_h]_j, j = 1, \dots, d$ denote the components of Φ_h. In view of $\Theta_h = \Phi_h^{-1} \circ \Psi$ the transformation formula for integrals yields

$$\begin{aligned}
\sum_{T\in\mathcal{T}_h^i} \int_{\Theta_h(T)} \left|\partial_{y_\nu}\partial_{y_\mu}\tilde{v}\right|^2 \,\mathrm{d}y &= \sum_{T\in\mathcal{T}_h^i} \int_{\Psi(T)} \left|(\partial_{y_\nu}\partial_{y_\mu}\tilde{v})\circ\Phi_h^{-1}(x)\right|^2 \det(\underline{A}^{-1}(x))\,\mathrm{d}x \\
&\lesssim \sum_{T\in\mathcal{T}_h^i}\sum_{j,k} \int_{\Psi(T)} |(\partial_j\partial_k v(x)|^2 \left|\partial_\nu[\Phi_h]_j(\Phi_h^{-1}(x))\partial_\mu[\Phi_h]_k(\Phi_h^{-1}(x))\right|^2 \,\mathrm{d}x \\
&\quad + \sum_{T\in\mathcal{T}_h^i}\sum_{k=1}^{d} \int_{\Psi(T)} |\partial_k v(x)|^2 \left|\partial_\nu\partial_\mu[\Phi_h]_k(\Phi_h^{-1}(x))\right|^2 \,\mathrm{d}x \\
&\lesssim \sum_{|\alpha|\leqslant 2}\sum_{T\in\mathcal{T}_h^i} \int_{\Psi(T)} |D_x^\alpha v|^2 \,\mathrm{d}x,
\end{aligned}$$

where we applied the bounds for the second derivatives from Lemma 2.2(b) on $\Phi_h^{-1}\circ\Psi(T) = \Theta_h(T)$ and (2.8). ∎

Proof of Lemma 2.5. We recall from [34, eq. (3.40)] that the measures $\mathrm{d}S_\Gamma$ on Γ and $\mathrm{d}S_{\Gamma_h}$ on Γ_h are related as follows:

$$\mathrm{d}S_\Gamma = \det(\underline{A}) \left\|\underline{A}^{-T} n_{\Gamma_h}\right\|_2 \mathrm{d}S_{\Gamma_h}, \quad \mathrm{d}S_{\Gamma_h} = \det(\underline{A}^{-1}) \left\|\underline{A}^T n_\Gamma\right\|_2 \mathrm{d}S_\Gamma. \tag{B.3}$$

(a) We will only show the result for the gradient. Using $(\nabla v)\circ\Phi_h = \underline{A}^{-T}\nabla\tilde{v}$ and the transformation rule (B.3) for the measure yields

$$\int_\Gamma |\nabla v|^2 \,\mathrm{d}S_\Gamma = \int_{\Gamma_h} \left|\underline{A}^{-T}\nabla\tilde{v}\right|^2 \det(\underline{A}) \left\|\underline{A}^{-T} n_{\Gamma_h}\right\|_2 \mathrm{d}S_{\Gamma_h} \lesssim \int_{\Gamma_h} |\nabla\tilde{v}|^2 \,\mathrm{d}S_{\Gamma_h},$$

where the last inequality follows from[8] equation (2.8). The reverse estimate is obtained in the same way by transforming from Γ_h to Γ and appealing to equations (2.7)–(2.8). The situation is similar in (b) and (c) where we will likewise only show one of the directions.

(b) Using $\underline{A}^T\nabla v = (\nabla\tilde{v})\circ\Phi_h^{-1}$ and the transformation rule (B.3) gives

$$\begin{aligned}
\int_{\Gamma_h} \|\nabla\tilde{v}\cdot n_{\Gamma_h}\|_2^2 \,\mathrm{d}S_{\Gamma_h} &= \int_\Gamma \left\|\underline{A}^T\nabla v\cdot(n_{\Gamma_h}\circ\Phi_h^{-1})\right\|_2^2 \det(\underline{A}^{-1}) \left\|\underline{A}^T n_\Gamma\right\|_2 \mathrm{d}S_\Gamma \\
&\lesssim \int_\Gamma \left[\left\|\underline{A}^T\nabla v\cdot(n_{\Gamma_h}\circ\Phi_h^{-1} - n_\Gamma)\right\|_2 + \left\|(\underline{A}^T - I)\nabla v\cdot n_\Gamma\right\|_2\right]^2 \left|\det(\underline{A}^{-1})\right| \left\|\underline{A}^T n_\Gamma\right\|_2 \mathrm{d}S_\Gamma \\
&\quad + \int_\Gamma \|\nabla v\cdot n_\Gamma\|_2^2 \left|\det(\underline{A}^{-1})\right| \left\|\underline{A}^T n_\Gamma\right\|_2 \mathrm{d}S_\Gamma \\
&\lesssim h^{2q}\|\nabla v\|_\Gamma^2 + \|\nabla v\cdot n_\Gamma\|_\Gamma^2,
\end{aligned}$$

where Lemma 2.3(b), equation (2.7) and (2.8) were employed in the last step.

[8] Note that (2.8) makes a statement about L^∞-norms in the volume whereas the integral is defined on a hypersurface. To pass from one to the other, we write the latter as sum of integrals over $\Theta_h(\Gamma_T), T\in\mathcal{T}^\Gamma$. Using $\Phi_h \in [C^{q+1}(\Theta_h(\mathcal{T}_h))]^d$ then allows to estimate the L^∞-norms on $\Theta_h(\Gamma_T)$ by the volumetric norms on $\Theta_h(T)$.

(c) Writing $P_{\Gamma_h}\circ\Phi_h^{-1}\underline{A}^T = P_{\Gamma_h}\circ\Phi_h^{-1}(\underline{A}^T - I) + (P_{\Gamma_h}\circ\Phi_h^{-1} - P_\Gamma) + P_\Gamma$ we deduce the claim from Lemma 2.3(c), equation (2.7) and (2.8):

$$\begin{aligned}\int_{\Gamma_h}\|\nabla_{\Gamma_h}\tilde{v}\|_2^2\,\mathrm{d}S_\Gamma &= \int_\Gamma \left\|P_{\Gamma_h}\circ\Phi_h^{-1}\underline{A}^T\nabla v\right\|_2^2 \det(\underline{A}^{-1})\left\|\underline{A}^T n_\Gamma\right\|_2\,\mathrm{d}S_\Gamma\\ &\lesssim \int_\Gamma\left[\left\|P_{\Gamma_h}\circ\Phi_h^{-1}(\underline{A}^T - I)\nabla v\right\|_2 + \left\|(P_{\Gamma_h}\circ\Phi_h^{-1} - P_\Gamma)\nabla v\right\|_2\right]^2\left|\det(\underline{A}^{-1})\right|\left\|\underline{A}^T n_\Gamma\right\|_2\,\mathrm{d}S_\Gamma\\ &\quad + \int_\Gamma\|P_\Gamma\nabla v\|_2^2\left|\det(\underline{A}^{-1})\right|\left\|\underline{A}^T n_\Gamma\right\|_2\,\mathrm{d}S_\Gamma\\ &\lesssim h^{2q}\|\nabla v\|_\Gamma^2 + \|\nabla_\Gamma v\|_\Gamma^2\,.\end{aligned}$$

■

Proof of Lemma 2.6.

(a) Let $\gamma(s) := f(s\Phi_h^{-1}(x) + (1-s)x)$ for $s\in[0,1]$ and $x\in M$. We have

$$\begin{aligned}f\circ\Phi_h^{-1}(x) - f(x) = \int_0^1\gamma'(s)\mathrm{d}s &= \int_0^1(\nabla f(s\Phi_h^{-1}(x) + (1-s)x), \Phi_h^{-1}(x) - x)\,\mathrm{d}s\\ &\lesssim \|\nabla f\|_{\infty,U}\left\|\Phi_h^{-1}(x) - x\right\|_2.\end{aligned}$$

Hence, we obtain from Lemma 2.1 that

$$\left\|f\circ\Phi_h^{-1} - f\right\|_M \lesssim \sqrt{|M|}\,\|\nabla f\|_{\infty,U}\left\|\Phi_h^{-1} - \mathrm{id}\right\|_{\infty,\Omega} \lesssim h^{q+1}\sqrt{|M|}\,\|\nabla f\|_{\infty,U}\,.$$

(b) We have

$$\begin{aligned}\left\|\nabla(f\circ\Phi_h^{-1} - f)\right\|_M &= \left\|\underline{A}^{-T}\nabla f\circ\Phi_h^{-1} - \nabla f\right\|_M\\ &\lesssim \left\|(\underline{A}^{-T} - I)[(\nabla f\circ\Phi_h^{-1} - \nabla f) + \nabla f] + (\nabla f\circ\Phi_h^{-1} - \nabla f)\right\|_M\\ &\lesssim \left(\left\|\underline{A}^{-T} - I\right\|_{\infty,M} + 1\right)\left\|\nabla f\circ\Phi_h^{-1} - \nabla f\right\|_M + \left\|\underline{A}^{-T} - I\right\|_{\infty,M}\|\nabla f\|_M\\ &\lesssim h^{q+1}\sqrt{|M|}\,\|f\|_{W^{2,\infty}(U)} + h^q\,\|\nabla f\|_M\,,\end{aligned}$$

where part (a) was employed to estimate the first term and we used (2.8) to obtain the bound for the second term.

(c) By the chain rule we have

$$\begin{aligned}\partial_{x_\nu}\partial_{x_\mu}(f\circ\Phi_h) = (\partial_\nu\partial_\mu f)\circ\Phi_h + (\partial_\nu\partial_\mu f)\circ\Phi_h(\partial_{x_\mu}[\Phi_h]_\mu - 1) + (\partial_\nu\partial_\mu f)\circ\Phi_h(\partial_{x_\nu}[\Phi_h]_\nu - 1)\partial_{x_\mu}[\Phi_h]_\mu\\ + \sum_{(i,j)\neq(\mu,\nu)}(\partial_j\partial_i f)\circ\Phi_h\partial_{x_\nu}[\Phi_h]_j\partial_{x_\mu}[\Phi_h]_i + \sum_i(\partial_i f)\circ\Phi_h\partial_{x_\nu}\partial_{x_\mu}[\Phi_h]_i,\end{aligned}\tag{B.4}$$

where $[\Phi_h]_i$ denotes the i-th component of Φ_h. According to Lemma 2.1 we have

$$\left\|\partial_{x_j}[\Phi_h]_i\right\|_{\infty,\Omega}\lesssim h^q \text{ for } i\neq j,\quad \left\|\partial_{x_j}[\Phi_h]_j - 1\right\|_{\infty,\Omega}\lesssim h^q \text{ for } j=1,\dots,d.$$

Combining this with the bounds for the second derivatives from Lemma 2.2 on $M=\Theta_h(T)$ yields

$$\begin{aligned}&\|\partial_{x_\nu}\partial_{x_\mu}(f\circ\Phi_h) - \partial_{x_\nu}\partial_{x_\mu}f\|_M\\ &\quad\lesssim \|(\partial_{x_\nu}\partial_{x_\mu}f)\circ\Phi_h - \partial_{x_\nu}\partial_{x_\mu}f\|_M + \sqrt{|M|}\left(h^q\,\|f\|_{W^{2,\infty}(V)} + h^{q-1}\,\|f\|_{W^{1,\infty}(V)}\right)\\ &\quad\lesssim h^{q-1}\sqrt{|M|}\,\|f\|_{W^{3,\infty}(V)}\,,\end{aligned}$$

where part (a) was once again applied in the last step.

(d) If we precompose equation (B.4) with Φ_h^{-1} we obtain

$$\begin{aligned}\partial_{x_\nu}\partial_{x_\mu}(f\circ\Phi_h)\circ\Phi_h^{-1} - \partial_{x_\nu}\partial_{x_\mu}f \\ = (\partial_\nu\partial_\mu f)(\partial_{x_\nu}[\Phi_h]_\nu\circ\Phi_h^{-1}-1)\partial_{x_\mu}[\Phi_h]_\mu\circ\Phi_h^{-1} + (\partial_\nu\partial_\mu f)(\partial_{x_\mu}[\Phi_h]_\mu\circ\Phi_h^{-1}-1) \\ + \sum_{(i,j)\neq(\mu,\nu)}(\partial_j\partial_i f)\partial_{x_\nu}[\Phi_h]_j\circ\Phi_h^{-1}\partial_{x_\mu}[\Phi_h]_i\circ\Phi_h^{-1} + \sum_i(\partial_i f)\partial_{x_\nu}\partial_{x_\mu}[\Phi_h]_i\circ\Phi_h^{-1}.\end{aligned}$$

Since the term $\partial_{x_\nu}\partial_{x_\mu}f$ is now on the left hand side of the equation, it is no longer necessary to appeal to part (a) to estimate this term. We can directly apply Lemma 2.1 to estimate the first order derivatives of Φ_h and Lemma 2.2 to obtain bounds for the second order derivatives on $\Phi_h^{-1}\circ\Psi(T) = \Theta_h(T)$. Hence,

$$\left\|\partial_{x_\nu}\partial_{x_\mu}(f\circ\Phi_h)\circ\Phi_h^{-1} - \partial_{x_\nu}\partial_{x_\mu}f\right\|_{\Psi(T)} \lesssim h^q\|f\|_{H^2(\Psi(T))} + h^{q-1}\|\nabla f\|_{\Psi(T)}$$

follows. ∎

Acknowledgements

We would like to thank Mihai Nechita for valuable input on the interface finite element formulation.

References

[1] Giovanni Alessandrini, Luca Rondi, Edi Rosset, and Sergio Vessella. The stability for the Cauchy problem for elliptic equations. *Inverse Probl.*, 25(12): article no. 123004 (47 pages), 2009.

[2] Nick Alger, Umberto Villa, Tan Bui-Thanh, and Omar Ghattas. A data scalable augmented Lagrangian KKT preconditioner for large-scale inverse problems. *SIAM J. Sci. Comput.*, 39(5):A2365–A2393, 2017.

[3] Christine Bernardi. Optimal Finite-Element Interpolation on Curved Domains. *SIAM J. Numer. Anal.*, 26(5):1212–1240, 1989.

[4] Thomas Boiveau, Erik Burman, Susanne Claus, and Mats Larson. Fictitious domain method with boundary value correction using penalty-free Nitsche method. *J. Numer. Math.*, 26(2):77–95, 2018.

[5] Muriel Boulakia, Erik Burman, Miguel A. Fernández, and Colette Voisembert. Data assimilation finite element method for the linearized Navier–Stokes equations in the low Reynolds regime. *Inverse Probl.*, 36(8): article no. 085003 (22 pages), 2020.

[6] Erik Burman. Stabilized Finite Element Methods for Nonsymmetric, Noncoercive, and Ill-Posed Problems. Part I: Elliptic Equations. *SIAM J. Sci. Comput.*, 35(6):A2752–A2780, 2013.

[7] Erik Burman, Susanne Claus, Peter Hansbo, Mats Larson, and André Massing. CutFEM: discretizing geometry and partial differential equations. *Int. J. Numer. Methods Eng.*, 104(7):472–501, 2015.

[8] Erik Burman, Guillaume Delay, and Alexandre Ern. A Hybridized High-Order Method for Unique Continuation Subject to the Helmholtz Equation. *SIAM J. Numer. Anal.*, 59(5):2368–2392, 2021.

[9] Erik Burman and Alexandre Ern. An Unfitted Hybrid High-Order Method for Elliptic Interface Problems. *SIAM J. Numer. Anal.*, 56(3):1525–1546, 2018.

[10] Erik Burman, Ali Feizmohammadi, Arnaud Münch, and Lauri Oksanen. Space time stabilized finite element methods for a unique continuation problem subject to the wave equation. *ESAIM, Math. Model. Numer. Anal.*, 55:S969–S991, 2021.

[11] Erik Burman, Ali Feizmohammadi, Arnaud Münch, and Lauri Oksanen. Spacetime finite element methods for control problems subject to the wave equation. *ESAIM, Control Optim. Calc. Var.*, 29: article no. 41 (40 pages), 2023.

[12] Erik Burman, Johnny Guzmán, Manuel A Sánchez, and Marcus Sarkis. Robust flux error estimation of an unfitted Nitsche method for high-contrast interface problems. *IMA J. Numer. Anal.*, 38(2):646–668, 2017.

[13] Erik Burman, Peter Hansbo, and Mats Larson. A cut finite element method with boundary value correction. *Math. Comput.*, 87(310):633–657, 2018.

[14] Erik Burman, Peter Hansbo, and Mats Larson. Solving ill-posed control problems by stabilized finite element methods: an alternative to Tikhonov regularization. *Inverse Probl.*, 34(3): article no. 035004, 2018.

[15] Erik Burman, Mihai Nechita, and Lauri Oksanen. Unique continuation for the Helmholtz equation using stabilized finite element methods. *J. Math. Pures Appl.*, 129:1–22, 2019.

[16] Erik Burman, Mihai Nechita, and Lauri Oksanen. A stabilized finite element method for inverse problems subject to the convection–diffusion equation. I: diffusion-dominated regime. *Numer. Math.*, 144(3):451–477, 2020.

[17] Erik Burman, Mihai Nechita, and Lauri Oksanen. A stabilized finite element method for inverse problems subject to the convection–diffusion equation. II: convection-dominated regime. *Numer. Math.*, 150(3):769–801, 2022.

[18] Erik Burman and Janosch Preuss. Reproduction material: Unique continuation for an elliptic interface problem using unfitted isoparametric finite elements. v2.

[19] Erik Burman and Janosch Preuss. Unique continuation for the Lamé system using stabilized finite element methods. *GEM. Int. J. Geomath.*, 14(1): article no. 9 (36 pages), 2023.

[20] Erik Burman and Paolo Zunino. A Domain Decomposition Method Based on Weighted Interior Penalties for Advection-Diffusion-Reaction Problems. *SIAM J. Numer. Anal.*, 44(4):1612–1638, 2006.

[21] Cătălin I. Cârstea and Jenn-Nan Wang. Propagation of smallness for an elliptic PDE with piecewise Lipschitz coefficients. *J. Differ. Equations*, 268(12):7609–7628, 2020.

[22] Zhiming Chen, Ke Li, and Xueshuang Xiang. An adaptive high-order unfitted finite element method for elliptic interface problems. *Numer. Math.*, 149(3):507–548, 2021.

[23] Wolfgang Dahmen, Harald Monsuur, and Rob Stevenson. Least squares solvers for ill-posed PDEs that are conditionally stable. *ESAIM, Math. Model. Numer. Anal.*, 57(4):2227–2255, 2023.

[24] Maksymilian Dryja. On Discontinuous Galerkin Methods for Elliptic Problems with Discontinuous Coefficients. *Comput. Methods Appl. Math.*, 3(1):76–85, 2003.

[25] Lars Eldén and Valeria Simoncini. A numerical solution of a Cauchy problem for an elliptic equation by Krylov subspaces. *Inverse Probl.*, 25(6): article no. 065002 (22 pages), 2009.

[26] Alexandre Ern, Annette F. Stephansen, and Paolo Zunino. A discontinuous Galerkin method with weighted averages for advection–diffusion equations with locally small and anisotropic diffusivity. *IMA J. Numer. Anal.*, 29(2):235–256, 2009.

[27] Gerald B Folland. *Real analysis: modern techniques and their applications*. Pure and Applied Mathematics. John Wiley & Sons, 2nd edition, 1999.

[28] Roland Glowinski, Chin-Hsien Li, and Jacques-Louis Lions. A numerical approach to the exact boundary controllability of the wave equation (I) Dirichlet controls: Description of the numerical methods. *Jpn. J. Appl. Math.*, 7:1–76, 1990.

[29] Jörg Grande, Christoph Lehrenfeld, and Arnold Reusken. Analysis of a High-Order Trace Finite Element Method for PDEs on Level Set Surfaces. *SIAM J. Numer. Anal.*, 56(1):228–255, 2018.

[30] Anita Hansbo and Peter Hansbo. An unfitted finite element method, based on Nitsche's method, for elliptic interface problems. *Comput. Methods Appl. Mech. Eng.*, 191(47-48):5537–5552, 2002.

[31] Christoph Lehrenfeld. High order unfitted finite element methods on level set domains using isoparametric mappings. *Comput. Methods Appl. Mech. Eng.*, 300:716–733, 2016.

[32] Christoph Lehrenfeld. A Higher Order Isoparametric Fictitious Domain Method for Level Set Domains. In Stéphane P. A. Bordas, Erik Burman, Mats Larson, and Maxim A. Olshanskii, editors, *Geometrically Unfitted Finite Element Methods and Applications*, pages 65–92. Springer, 2017.

[33] Christoph Lehrenfeld, Fabian Heimann, Janosch Preuß, and Henry von Wahl. `ngsxfem`: Add-on to NGSolve for geometrically unfitted finite element discretizations. *J. Open Source Softw.*, 6(64): article no. 3237, 2021.

[34] Christoph Lehrenfeld and Arnold Reusken. Analysis of a high order unfitted finite element method for an elliptic interface problem. *IMA J. Numer. Anal.*, 38(3):1351–1387, 2018.

[35] Christoph Lehrenfeld and Arnold Reusken. L^2-estimates for a high order unfitted finite element method for elliptic interface problems. *J. Numer. Math.*, 27(2):85–99, 2019.

[36] Yimin Lou. *High-order Unfitted Discretizations for Partial Differential Equations Coupled with Geometric Flow*. PhD thesis, University of Göttingen, 2023.

[37] Kent-André Mardal, Bjørn Fredrik Nielsen, and Magne Nordaas. Robust preconditioners for PDE-constrained optimization with limited observations. *BIT*, 57:405–431, 2017.

[38] Ralf Massjung. An Unfitted Discontinuous Galerkin Method Applied to Elliptic Interface Problems. *SIAM J. Numer. Anal.*, 50(6):3134–3162, 2012.

[39] Siddhartha Mishra and Roberto Molinaro. Estimates on the generalization error of physics-informed neural networks for approximating PDEs. *IMA J. Numer. Anal.*, 43(1):1–43, 2023.

[40] Mihai Nechita. *Unique continuation problems and stabilised finite element methods*. PhD thesis, University College London, 2020.

[41] Arnold Reusken. Analysis of an extended pressure finite element space for two-phase incompressible flows. *Comput. Vis. Sci.*, 11(4):293–305, 2008.

[42] Luc Robbiano. Théorème d'unicité adapté au contrôle des solutions des problèmes hyperboliques. *Commun. Partial Differ. Equations*, 16(4-5):789–800, 1991.

[43] Joachim Schöberl. NETGEN An advancing front 2D/3D-mesh generator based on abstract rules. *Comput. Vis. Sci.*, 1(1):41–52, 1997.

[44] Joachim Schöberl. C++11 Implementation of Finite Elements in NGSolve. Technical report, ASC-2014-30, Institute for Analysis and Scientific Computing, 2014.

[45] Elias M. Stein. *Singular Integrals and Differentiability Properties of Functions*, volume 30 of *Princeton Mathematical Series*. Princeton University Press, 1971.

[46] Haijun Wu and Yuanming Xiao. An Unfitted *hp*-Interface Penalty Finite Element Method for Elliptic Interface Problems. *J. Comput. Math.*, 37(3):316–339, 2018.

[47] Yuanming Xiao, Jinchao Xu, and Fei Wang. High-order extended finite element methods for solving interface problems. *Comput. Methods Appl. Mech. Eng.*, 364: article no. 112964 (21 pages), 2020.

[48] Paolo Zunino, Laura Cattaneo, and Claudia Maria Colciago. An unfitted interface penalty method for the numerical approximation of contrast problems. *Appl. Numer. Math.*, 61(10):1059–1076, 2011.